Carboxymethyl Tamarind Kernel Gum/CuO-Based Nanocomposite Hydrogel in Oral Drug Delivery of Ciprofloxacin

A Dissertation Submitted

In Partial Fulfilment of the Requirements for the

Degree of

MASTER OF SCIENCE

in

CHEMISTRY

by

NANCY

(24/MSCCHE/29)

&

RAHUL PANWAR

(24/MSCCHE/35)

Under the Supervision of

Prof. S.G. WARKAR

Department of Applied Chemistry

DELHI TECHNOLOGICAL UNIVERSITY

(Formerly Delhi College of Engineering)

Shahbad Daulatpur, Main Bawana Road, Delhi-110042, India

June 2026

DELHI TECHNOLOGICAL UNIVERSITY

(Formerly Delhi College of Engineering)

Shahbad Daulatpur, Main Bawana Road, Delhi-110042, India

CANDIDATE'S DELCLARATION

We NANCY (24/MSCCHE/29) and Rahul Panwar (24/MSCCHE/35) hereby certify that the work which is being presented in the dissertation entitled **"Carboxymethyl Tamarind Kernel Gum/CuO-Based Nanocomposite Hydrogel in Oral Drug Delivery of Ciprofloxacin"** in partial fulfillment of the requirements for the award of Degree of Master of Science, submitted in the Department of Applied Chemistry, Delhi Technological University is an authentic record of our own work carried out during the period from November 2025 to May 2026 under the supervision of Prof. S.G. Warkar. The matter presented in the dissertation has not been submitted by us for the award of any other degree of this or any other Institute.

Nancy **Rahul Panwar**

(24/MSCCHE/29) **(24/MSCCHE/35)**

CERTIFICATE

Certified that Nancy (24/MSCCHE/29) and Rahul Panwar (24/MSCCHE/35) has carried out their research work presented in this dissertation entitled **"Carboxymethyl Tamarind Kernel Gum/CuO-Based Nanocomposite Hydrogel in Oral Drug Delivery of Ciprofloxacin"** for the award of Master of Science from Department of Applied Chemistry, Delhi Technological University, Delhi, under my supervision. The dissertation embodies results of original work, and studies are carried out by the students themselves and the contents of the dissertation do not form the basis for the award of any other degree to the candidate or to anybody else from this or any other University/ Institution.

PLACE – DELHI

DATE – 20/06/2026

Prof. S.G. Warkar

(SUPERVISOR)

DELHI TECHNOLOGICAL UNIVERSITY

(Formerly Delhi College of Engineering)

Shahbad Daulatpur, Main Bawana Road, Delhi-110042, India

PLAGIARISM VERIFICATION

Title of dissertation "**Carboxymethyl Tamarind Kernel Gum/CuO-Based Nanocomposite Hydrogel in Oral Drug Delivery of Ciprofloxacin.**"

This is to report that the above dissertation was scanned for similarity detection. Process and outcome are given below:

Software used: **Turnitin**

Similarity Index: **7%**

Total Word Count: **12082**

Date: **10 June 2026**

Nancy	**Rahul Panwar**	**Prof. S.G. Warkar**
(24/MSCCHE/29)	**(24/MSCCHE/35)**	**(Supervisor)**

ABSTRACT

Carboxymethyl tamarind kernel gum (CMTKG), bovine serum albumin (BSA), acrylamide (AAM) and Acrylic acid (AA) was combined to create a novel hydrogel system that included ciprofloxacin (CFX) as a model therapeutic agent. This study investigates CMTKG-g-poly(acrylamide-co-acrylic acid)/BSA hydrogel containing Phytogenic CuO nanoparticles for drug delivery of Ciprofloxacin. The free radical graft polymerization method is used to graft acrylamide and acrylic acid onto the Carboxymethyl tamarind kernel gum backbone. Lysine-coated CuO nanoparticles were synthesized using plant extract of *Madagascar periwinkle* that follows green synthesis. Various hydrogel compositions were synthesized with different compositions of Bovine serum albumin and nanoparticles. Swelling studies and drug release studies were conducted carefully at pH 2.2 and 7.4. According to swelling studies, it is observed that the hydrogel swelled more at pH 7.4 and less at pH 2.2. The Equilibrium swelling ratio of nanocomposite hydrogel was found to be (306-634) % in pH 2.2 and (1096-1210) % in pH 7.4. Subsequent examination of drug release revealed higher release at pH 2.2. Nanocomposite hydrogel shows drug release 59-62% in pH 2.2 and 40-50.5% in pH 7.4 in 7h. The Korsmeyer–Peppas model was found to be the best fit for the drug release profile based on kinetic evaluations. We added BSA and NPs to reduce the swelling and enhance the cross-linking in hydrogel network to overcome the burst release of the Ciprofloxacin and facilitate the controlled release of the drug. Hydrogels were characterized by following characterization techniques for the studies which are FTIR, PXRD, FESEM, Zeta Potential, Antimicrobial activity and MTT Assay. The particle size was found to be 26.23±2.95 using Debye-Scherrer equation. At a concentration of 80 µg/mL, antimicrobial assays showed significant inhibition. Inhibition zones of 10 mm against *E. coli* and 11 mm against *S. aureus* were shown by the Ciprofloxacin-loaded nanocomposite hydrogel. MTT assay was performed at 50-250 µg/mL concentration on L929 cell lines. The hydrogel's outstanding biocompatibility was confirmed that showed >90% cell viability. As a result, this hydrogel formulation shows great promise for improved cellular compatibility, bactericidal efficacy, and regulated drug delivery.

Keywords: Hydrogel drug delivery system, Controlled drug release, Ciprofloxacin (CFX), Antibacterial activity, Biocompatibility

DELHI TECHNOLOGICAL UNIVERSITY

(Formerly Delhi College of Engineering)

Shahbad Daulatpur, Main Bawana Road, Delhi-110042, India

AKNOWLEDGEMENTS

The success and outcome of this project required a lot of guidance and assistance from many people and we are extremely fortunate to have got this all along the completion of this project work.

We wish to express our gratitude towards my project supervisor, Prof. S.G. WARKAR, Department of Applied Chemistry, Delhi Technological University, who provided us with a golden opportunity to work under their able guidance. Their scholastic guidance and sagacious suggestions helped us to complete the project on time.

We wish to thank Prof. D. Kumar, Head of the Department of Applied Chemistry, at Delhi Technological University for his constant motivation.

We are particularly thankful to Ms. Rashmi Sharma for her extensive help in teaching me the fundamentals of techniques and for her patience in addressing our numerous questions throughout our research and her constant guidance and support. We are thankful for and fortunate enough to get constant encouragement, support, and guidance from all teaching staff of the Department of Applied Chemistry, which helped me in completing my project work

Finally, yet importantly, we would like to express our heartfelt thanks to our beloved parents and friends who have endured our long working hours and whose motivation kept us going.

Last but not least we want to thank ourselves for doing all the hard work.

Nancy & Rahul Panwar

CONTENTS

Table of Contents

LIST OF SCHEMES

LIST OF TABLES

LIST OF FIGURES

LIST OF ABBREVATIONS AND SYMBOLS

AAM	Acrylamide
PAM	Polyacrylamide
ATR-FTIR	Attenuated Total Reflection- Fourier Transform Infrared Spectroscopy
CMTKG	Carboxymethyl Tamarind Kernel Gum
BSA	Bovine Serum Albumin
HSA	Human Serum Albumin
AA	Acrylic Acid
PAA	Poly(acrylic acid)
PEG	Polyethyl glycol
COO^-	Carboxylate ion
$-CONH_2$	Amide group
$-NH_2$	Amine group
DEE	Drug Entrapment Efficiency
DLE	Drug Loading Efficiency
g	Gram
IPN	Interpenetrating Polymeric Hydrogel
KPS	Potassium per sulphate
MBA	N', N' -methylene-bis (acrylamide)
mg	Milligram
nm	Nanometer
OH	Hydroxyl group
PXRD	Powder X-ray diffraction
R^2	Regression coefficient

FESEM	Field Emission Scanning Electron Microscopy
UV-Vis	Ultraviolet- visible spectroscopy
W_d	Weight of dried hydrogel
W_s	Weight of swollen hydrogel
%	Percentage
λ_{max}	Maximum Wavelength

CHAPTER 1

INTRODUCTION

INTRODUCTION

Hydrogels are high water content, 3D networks of natural or synthetic polymers, with a high degree of flexibility[1]. They are ideal for use in a wide range of applications because they are soft, rubber-like, have a consistency similar to living tissues, and can hold a significant amount of water or biological fluids under physiological conditions. A hydrogel is sometimes referred to as a "smart" or "intelligent" material because it can sense stimuli and react by changing its chemical or physical characteristics, which causes the trapped drug to release under controlled conditions [2].

The presence of hydrophilic groups like -OH, -CONH, $-SO_3H$ and $-CONH_2$ in polymers that form hydrogel structures is responsible for their propensity to absorb water. Depending on the type, the polymer is thus hydrated to varying degrees (sometimes more than 90%wt.) due to the contribution of these groups and domains in the network.[2], [3]. The hydrophilic functionalities cross-linking offers structural stability and keeps the hydrophilic polymers from dissolving in the aqueous medium right away [4].

Important properties of hydrogels include stretchability, deformability, biocompatibility, softness, and toughness. Polymer-based hydrogels have found widespread application in drug delivery, food, cosmetics, contact lenses, corneal implants, tendons, ligaments, cartilage, and bone due to their exceptional hydrophilicity, permeability, compatibility, and low friction coefficient. Additionally, superporous hydrogels, a unique class of hydrogels, may find use as superdisintegrants, controlled release platforms, and gastroretentive drug delivery systems in both short- and long-term applications [5]. Here, we'll concentration on controlled oral Drug delivery.

1.1. Classification of Hydrogel:

Hydrogels have been classified into following different groups based on their origin, structure, preparation method, crosslinking mechanism, charge, responsive nature, physical aspect, and degradation [6].

- **Based on source**

Hydrogels can be broadly categorized into three groups based on their source: natural, semi-synthetic and synthetic.

a) **Natural hydrogels**- provides biocompatibility.

b) **Semi-synthetic hydrogels**- which have adjustable characteristics.
c) **Synthetic hydrogel**- which offers a high degree of variability [7].

- **Based on Composition**

The composition of hydrogels can be used to classify them into four categories, viz., homopolymeric, copolymeric, interpenetrating polymer network (IPN), and semi interpenetrating polymer network hydrogels (semi-IPN).

a) **Homopolymer Hydrogel**- The polymeric chains in homopolymer hydrogel are derived from one species of monomer [8].
b) **Copolymer hydrogels**- Copolymeric hydrogels are made up of two or more distinct monomer species with at least one hydrophilic component that are arranged along the polymer network's chain in an alternating, random, or block pattern [9].
c) **Interpenetrating Polymer Network (IPN)-** A polymer made up of two or more networks that are at least partially molecularly interlaced but not covalently bonded to one another, making it impossible to separate them without breaking chemical bonds. An IPN is not a combination of two or more pre-formed polymer networks [10], [11].
d) **Semi- Interpenetrating Polymer Network-** A polymer made up of one or more networks and one or more linear or branched polymers, where at least some of the linear or branched macromolecules penetrate at least one of the networks on a molecular scale [11], [12].

- **Based on Configuration**

Based on their configuration, hydrogels are divided into three groups. Depending on how they are arranged, hydrogels can be amorphous, crystalline, or semi-crystalline [3].

a) Amorphous- An amorphous polymer's molecular structure is entirely random, meaning that its molecular chains are entangled and oriented randomly with no discernible pattern.[13], [14].
b) **Crystalline-** The long range order is present in the crystalline structure [15].
c) **Semi-crystalline-** Both crystal line and amorphous phases make up semicrystalline polymers. Because they contain crystalline regions, their mechanical performance at high temperatures is frequently better than that of amorphous polymers [16], [17].

- **Based on Cross-linking**

Depending on whether the cross-link junctions are chemical or physical, hydrogels can be classified into two groups.

a) Chemically cross-linked networks- have permanent junctions.

b) **Physical networks**- have transient junctions that are caused by either polymer chain entanglements or physical interactions like hydrogen bonds, ionic interactions, or hydrophobic interactions [8].

- **Based on Ionic- Charge**

Based on whether there is an electrical charge on the cross-linked chains, hydrogels can be divided into four groups

a) Nonionic (neutral).
b) Ionic (including cationic or anionic).
c) Amphoteric electrolyte (ampholytic) that has both basic and acidic groups.
d) Zwitterionic (polybetaines) which have cationic and anionic groups in each structural repeating unit [18]

- **Hydrogels are categorized according to the mechanism governing the release of drugs:** .

a) Systems with diffusion-controlled release.

b) Systems for swelling controlled release.

c) Systems with chemically regulated release.

d) Systems that respond to the environment.

Carboxymethyl tamarind kernel gum (CMTKG)

Tamarind Kernel Gum (TKG), which is extracted from Tamarindus indica L seeds, is the source of CMTKG, a biopolymer. This polysaccharide is composed of galactose, xylose, and glucose in a 3:2:1 ratio. Its linear β-(1,4)-D glucose backbone has partial α-D-xylo-pyranose (C-1) substitution at the O glucopyranosyl (C-6) residues, which are then further substituted at C-2 by β-D galactopyranosyl units (C-1). Williamson's etherification (SN 2 mechanism) of TKG and alkaline mono-chloroacetic acid results in CMTKG, which has carboxymethyl groups

(-CH2COOH) at its C-6 position [19].

Carboxymethyl tamarind kernel gum (CMTKG), which has appropriate properties like broad pH tolerance, high drug loading capacity, hydrophilicity, and stability, is produced by chemically modifying TKG [20].

The antibacterial qualities of TKG are demonstrated by CMTKG. Tissue engineering, drug delivery, agriculture, paper, and textiles are just a few of the industries that can benefit from CMTKG's superior functional qualities. Over the past ten years, a thorough investigation into CMTKG as a drug delivery method has been conducted due to reliable data regarding its excellent pharmacological and physicochemical properties [21].

Bovine Serum Albumin (BSA)

With 76% similarity, BSA and HSA are the most frequently used protein models in biophysical and biochemical research in recent years [22].

According to the crystal structure analysis, BSA contains 582 amino acid residues, 20 tyrosyl residues (Tyr), and two tryptophan residues (Try), which are located in positions 134 (sub domain IA) and 212 (sub-domain IIA) [23].

The water-soluble nature of bovine serum albumin (BSA), which is crucial for interaction studies, has led to its selection[24] [22].

Numerous mononuclear and polynuclear Cu^{2+}, Ni^{2+}, Zn^{2+}, Co^{2+} and Pt^{2+} complexes with aromatic ligands—some of which have known pharmacologically active moieties—have been studied for their BSA interaction and binding capacity [22].

Polyacrylamide

PAM is composed of repeating units of the acrylamide (AM)[25]. The non-toxic, pH-sensitive polymer polyacrylamide (PAM) is well known for its exceptional biocompatibility. It has the –CONH2 group, which allows for flexible swelling and drug release behaviours at various pH levels [26]. PAM-based hydrogels exhibit mechanical resilience and the ability to maintain their shape. To create composite hydrogels with exceptional qualities, they have been widely mixed with synthetic and natural polymers like carboxymethyl cellulose and carboxymethyl tamarind kernel gum [27].

Poly(acrylic acid)

Acrylic acid polymerises to form Poly(acrylic acid). The following equation illustrates how the

PAA chains can absorb and hold onto water molecules when water at neutral pH is present because they will lose their protons and gain a negative charge [28]

$$n\ CH_2=CH-CO_2H+H_2O \xrightarrow{pH=7.0} n\ CH_2=CH-H_2O+COOH \quad (1)$$

***Madagascar periwinkle* plant**

Vinca rosea, *Ammocallis rosea*, and *Lochnera rosea* are some synonyms for *Catharanthus roseus L*. It is a significant Apocynaceae medicinal plant with a wealth of beneficial alkaloids that are used to treat menstrual issues, diabetes, blood pressure, asthma, constipation, and cancer of thousands of patients, both due to their efficacy and distinct mode of action. The plant has long been used in traditional Chinese medicine, Ayurvedic medicine, and other medical systems. In the 20th century, Western medical researchers started studying Catharanthus roseus and its extracts, discovering a number of compounds that could be used to treat cancer. The dried root, leaves, flowers, and stalks of the plant have all been utilized in local herbal medicine. The entire dried plant is used to extract alkaloids for use in contemporary medicine [29].

MP is available in a wide range of styles and hues, from the original pink to white, hot pink, purple, and mauve [30].

Additionally, we used MP leaves that have purple flowers, or "rosea." Two types of PM—rosea and alba—have been the subject of numerous studies. All of the findings showed that rosea performs better overall than alba. Rosea fared much better under water stress than alba because it has more antioxidant activity and a higher alkaloid content in its leaves and roots [31].

Copper Oxide Nanoparticles

It is commonly known that the properties of nanoparticles are superior to those of their bulk counterparts. Particle size and specific surface area are inversely correlated. Because of their larger surface area, nanoparticles are therefore used to increase the rates of interfacial processes. As a result, nanoparticles are superior adsorbents and catalysts. With intended uses in numerous scientific and technological domains, the need for nanomaterials is constantly growing. Green nanomaterial synthesis has garnered a lot of interest. Green synthesis frequently makes use of plant extracts with therapeutic value. Few components of plant extracts with therapeutic value are thought to be included in the synthesis of nanoparticles [32]. We have followed similarly.

CuO NPs amalgamation has been considered superior to other metal oxide nanoparticles due to their enormous potential applications over the past ten year [33].

Due to their wide range of uses. They have superior antibacterial effects without compromising the material's mechanical qualities because of their higher surface-to-volume ratio and smaller particle size. Co-precipitation, sol-gel, hydrothermal, and other techniques can be used to create copper oxide nanoparticles. These techniques, however, have a number of disadvantages, such as inconsistent particle sizes, the use of dangerous chemicals, high costs, and substantial energy consumption. A simpler, more affordable, and ecologically friendly green synthesis technique that uses plant secondary metabolites as capping agents has been developed to overcome these constraints [34] Through coordination bonds or electron donation, plant functional groups interact with metal ions on the surface of nanoparticles in green synthesis techniques [11]. Capping agents are frequently used in colloidal dispersions to precisely control the growth, agglomeration, and physicochemical properties of nanoparticles. Consequently, their antibacterial activity is enhanced by keeping the particle size within the nanoscale range [34]. The PEG was also added to prevent the aggregation of nanoparticles and for their better dispersion [35].

Ciprofloxacin

A second-generation broad-spectrum antibiotic, ciprofloxacin (CFX) exhibits encouraging outcomes because of its improved pharmacokinetic activity and efficient treatment of a number of dangerous infections [36].

CFX is a broad-spectrum antimicrobial fluoroquinolone that is clinically recommended for the treatment of bacterial infections, including infectious diarrhea, typhoid fever, acute uncomplicated cystitis in females, chronic bacterial prostatitis, urinary and lower respiratory tract infections, acute sinusitis and skin-related infections, bone and joint infections, and uncomplicated cervical and urethra gonorrhea. The gastrointestinal tract absorbs it at a high rate. The permeability of this medication varies with concentration[37].

To the best of our knowledge, carboxymethyl tamarind kernel gum (CMTKG) is being used for the first time with BSA and Lysine-coated CuO nanoparticles. This work involves synthesis, characterization, swelling studies, drug release experiment, and the kinetic modelling of Ciprofloxacin released from CMTKG-g-poly(acrylamide-co-acrylic acid)/BSA/CuO nanocomposite hydrogels.

Biodegradable polymeric hydrogels are represented as an excellent drug delivery system to fine-tuned drug release profile as per clinical necessity. However, the direct incorporation of drug molecules into the hydrogel matrix has been reported with very high initial burst release profile followed by the short-term slow release profile. In addition, this burst release could go beyond 70% of the total drug loading, consequently, the smaller amount of drug available for the prolonged release. Ultimately, a problem of antibiotic resistance may appear.

This research delves into the fabrication of CFX-loaded CMTKG-g-poly(acrylamide-co-acrylic acid)/BSA/CuO nanocomposite hydrogel, aiming for a pH-dependent, slow and controlled release of the drug CFX via oral drug delivery.

Characterization techniques such as PXRD, ATR-FTIR, FESEM were employed to assess the hydrogels. Additionally, the study investigates how varying amounts of BSA and CuO NPs have an impact on the hydrogel's swelling behaviour in pH 2.2 and 7.4 buffers. Additionally, a variety of mathematical models, including Korsmeyer-Peppas, Higuchi, Zero order, and First order, were used to assess the drug release kinetics.

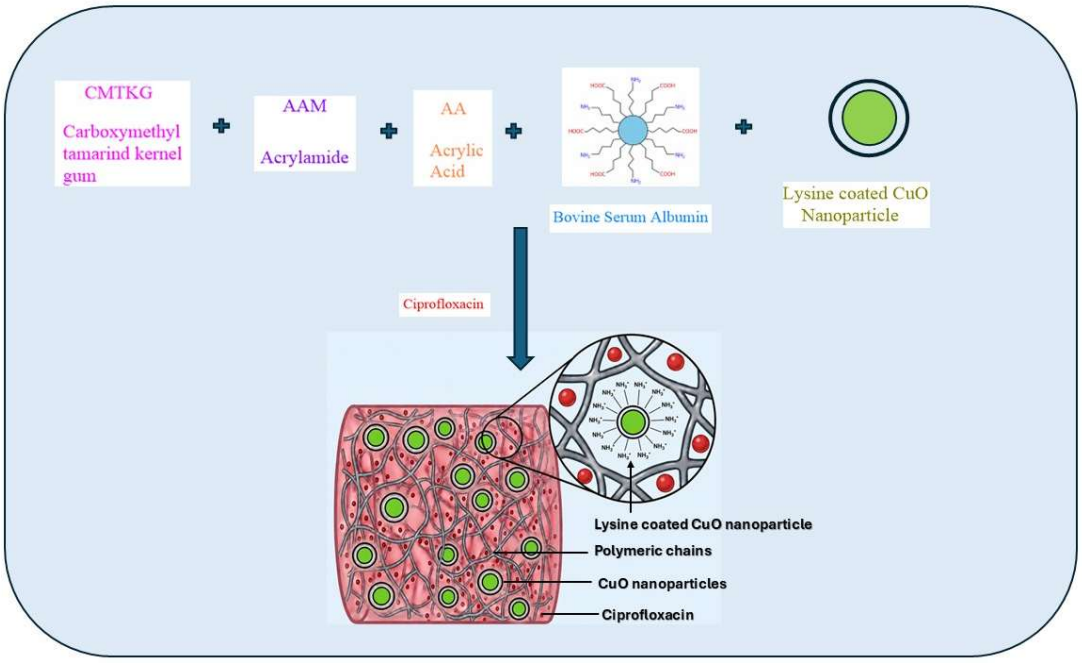

Fig 1.1 CFX-loaded CMTKG-g-poly(acrylamide-co-acrylic acid)/BSA/CuO nanocomposite hydrogel matrix.

CHAPTER 2

LITERATURE SURVEY

LITERATURE SURVEY

Hydrogel Material	Crosslinker	NPs	Drug	Reference
CMTKG/Poly(sodium acrylate)	PEGDA	ZnO	Ciprofloxacin	[38]
PAM/MMT/CMC/MgO	MBA	MgO	Acyclovir	[39]
CMC and PEG	DA-PEG	Tannic acid	Antagomir-21	[40]
Alginate	Cystine/$CaCl_2$	Fe_3CO_4	Doxorubicin	[41]
Hyaluronic acid	HS-MMP-SH	Copper Sulphide	Deferoxamine	[42]
Guggal gum/PAM	MBA	SrO-CoO	Naproxen	[43]

2.1 CMTKG/Poly(sodium acrylate) – PEGDA – ZnO – Ciprofloxacin

The foundation of this system is carboxymethyl tamarind kernel gum (CMTKG), a naturally occurring polysaccharide that has been chemically modified. It is copolymerized with poly(sodium acrylate) and crosslinked using poly(ethylene glycol) diacrylate (PEGDA) via free-radical polymerization. To transport and release the broad-spectrum fluoroquinolone antibiotic ciprofloxacin, zinc oxide nanoparticles that were individually synthesized using a hydrothermal method were incorporated into this network.

2.2 PAM/MMT/CMC/MgO – MBA – MgO – Acyclovir

This formulation combines polyacrylamide (PAM) with carboxymethyl cellulose (CMC) and montmorillonite (MMT) nanoclay, crosslinked through N,N′-methylenebisacrylamide (MBA), with magnesium oxide (MgO) nanoparticles dispersed through the network. Montmorillonite is a layered aluminosilicate clay that is frequently used as a nanofiller in hydrogel composites. Its large surface area and high aspect ratio both create convoluted diffusion pathways that slow solute transport and mechanically reinforce the polymer network. Acylovir is used as model

drug here.

2.3 CMC and PEG – DA-PEG – Tannic Acid – Antagomir-21

In this system, polyethylene glycol (PEG) and carboxymethyl cellulose (CMC) are crosslinked via dialdehyde-functionalized PEG (DA-PEG), which reacts with free amine or hydroxyl groups on the polysaccharide backbone through dynamic covalent (Schiff-base/acetal-type) linkages, giving the network injectable and self-healing properties. Instead of using a traditional inorganic nanoparticle, tannic acid, a naturally occurring polyphenol rich in catechol and pyrogallol groups, is added as the nanoscale functional filler. The resulting nanocomposite hydrogel act as drug delivery platform for Antagomir-21.

2.4 Alginate – Cystamine/$CaCl_2$ – Fe_3O_4 – Doxorubicin

Due to its simple ionic gelation with divalent cations, sodium alginate is one of the most widely used natural polysaccharides in drug-delivery hydrogels. The alginate network in this system is doubly crosslinked: cystamine, a small molecule with a central disulfide bond, introduces a redox-cleavable covalent crosslink, while $CaCl_2$ provides the classical ionic crosslinking between alginate's carboxylate groups and Ca^{2+} ions. Because it can be selectively cleaved in the reducing, glutathione-rich intracellular environment typical of many tumor cells, this disulfide linkage is important because it gives the hydrogel a degree of redox-responsive, tumor-selective degradation. This crosslinked alginate matrix contains embedded magnetite (Fe3O4) superparamagnetic nanoparticles that can be used as an MRI contrast agent to monitor carrier distribution, as well as to reinforce the gel and enable magnetically guided localization or triggered drug release under an external magnetic field. This redox- and magnetically responsive alginate/Fe3O4 hydrogel is loaded with the chemotherapeutic doxorubicin, an anthracycline commonly used against solid tumors but linked to dose-limiting cardiotoxicity.

2.5 Hyaluronic Acid – HS-MMP-SH – Copper Sulphide – Deferoxamine

Due to its inherent biocompatibility, biodegradability, and capacity to interact with CD44 receptors, which are overexpressed on numerous tumor and inflammatory cell types, hyaluronic acid (HA), a naturally occurring glycosaminoglycan that is prevalent in the extracellular matrix, is a popular hydrogel backbone for biomedical applications. A thiol–thiol (–SH – HS–) linkage based on a matrix metalloproteinase (MMP)-cleavable peptide sequence (referred to as HS-MMP-SH) crosslinks the HA network in this system. Because MMPs are overexpressed in tumor stroma and chronic wound environments, this design makes the

hydrogel enzyme-responsive. MMPs can hydrolyze the embedded peptide crosslinker, causing the gel to disassemble locally and release its payload only at locations where MMP activity is elevated. The encapsulated agent, deferoxamine, is an iron-chelating drug.

2.6 Guggal Gum/PAM – MBA – SrO-CoO – Naproxen

Guggal gum (gum guggul), a plant-derived polysaccharide exudate, is used in this final system. It is copolymerized with polyacrylamide (PAM) and crosslinked with N,N′-methylenebisacrylamide (MBA), the same crosslinking chemistry, demonstrating MBA's wide range of applications as an inexpensive, covalent vinyl crosslinker for acrylamide-based hydrogel networks created by free-radical polymerization. This matrix contains a mixed strontium oxide–cobalt oxide (SrO–CoO) nanoparticle filler. Naproxen, the loaded medication, is a non-steroidal anti-inflammatory drug (NSAID) that is frequently used to treat pain and inflammation in diseases like rheumatoid arthritis and osteoarthritis.

Our review of current literature shows a variety of hydrogel materials with their model drug. However, our survey highlighted a specific need for more robust, controlled and dual finctional platform that combines natural gum with green synthesized metal oxides specifically for Ciprofloxacin delivery.

CHAPTER 3

MATERIAL AND SYNTHESIS

3.1 Materials

Carboxymethyl tamarind kernel gum (CMTKG) having a molecular weight (MW = 9.14×10^5 g mol^{-1}) was generously provided by Hindustan gum (Bhiwani, India), Acrylamide (AAM), Acrylic Acid (AA), potassium persulphate (KPS) and *N*, *N*′-methylenebisacrylamide (MBA), $CuCl_2$ were received from the Merck, Germany. Ciprofloxacin was obtained from M/S Unicure, India. Buffer solutions of pH 2.2 and 7.4 were made in lab. Distilled water was used for all the experiments.

3.2. Preparation of Plant Extract

Madagascar periwinkle plant leaves were collected from garden and washed properly to remove the dirt and impurities from the leaves. The leaves were left for drying. Solvent Extraction method was used to get the plant extract. The dried leaves were then emersed in 100 ml of ethanol for around 30 min that was followed by addition of 100 ml water to it. Then the mixture was left for boiling for around 2h at 60°C. Later the filtration process was performed using Whatman filter paper. The filtrate was kept in refrigerator at 4-6°C for future use [44].

3.3. Synthesis of Lysine-coated CuO Bio-Nanoparticles

CuO NPs were effectively produced from *Madagascar periwinkle* plant extract. 200 ml plant of 10 M $CuCl_2$ aqueous solution was prepared. Then, 0.4g lysine was added followed by addition of 10 ml plant extract. NaOH was used to lower down the pH to 10. The mixture was continuously stirred for 3h at 60°C. This resulted in formation of black suspension. The suspension was further heated for 1 h at 80°C. Whatman filter paper used to filter the lysine-coated CuO NPs from filtrate. Then, it was left for drying in an oven for 24h and stored for later use [45].

Fig 3.1 Synthesis of Lysine-coated CuO Nanoparticles.

3.4. Synthesis of CMTKG-g-poly(AAM-co-AA)/BSA composite hydrogel

The free radical polymerization technique is used to prepare the CMTKG-g-poly(acrylamide-co-acrylic acid)/BSA hydrogel. 0.3g of CMTKG was mixed in 7 ml distilled water and left for complete dissolution for 1h with continuous stirring at 470 rpm. Aqueous solution of BSA was then added in dissolved CMTKG solution. 10 min later, 0.4g acrylamide was added and left for stirring for 30 min. After that 20 µl acrylic acid was added and after 10 min the KPS was added followed by addition of MBA. Polymerization process was carried out for 10 min. The product was transferred into test tube for hot water bath for 15 min at 80°C. After that, the gel was cut into equal sized discs. The synthesised hydrogel was then dispersed into distilled water to eliminate the unreacted monomers for 5 h. After that, the formed hydrogel was left in an incubator for drying at room temperature [46].

The composition of used substituents is shown in the table below:

Table 1.

Sample Name	Composition Ratio					
	CMTKG	BSA	ACRYLAMIDE	ACRYLIC ACID	MBA	KPS
B0	0.3g	0	0.4g	20µl	0.020g	0.028g
B1	0.3g	0.1g	0.4g	20µl	0.020g	0.028g
B2	0.3g	0.2g	0.4g	20µl	0.020g	0.028g
B3	0.3g	0.3g	0.4g	20µl	0.020g	0.028g

3.5 Preparation of CMTKG-g-poly(AAM-co-AA)/BSA/CuO nanocomposite hydrogel

A range of nanocomposite hydrogels were produced by adding various amounts of CuO NPs. CuO NPs were weighed in different quantities- 5mg, 10 mg and 20 mg and were dispersed in PEG/water mixture. The mixture was left for stirring for 30 min to get homogeneous mixture. The MBA and KPS were added afterwards [38].

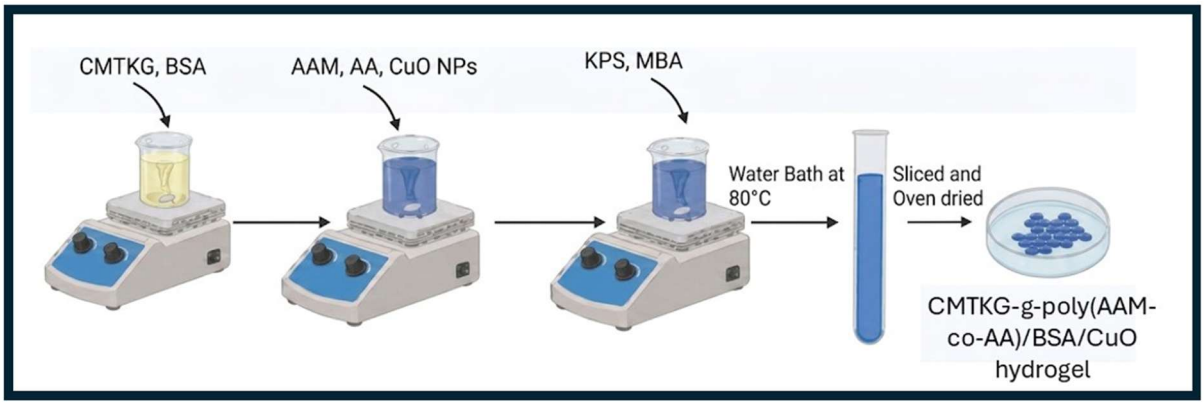

Fig 3.2 Synthesis of CMTKG-g-poly(AAM-co-AA)/BSA/CuO nanocomposite hydrogel.

Table 2.

Sample code		**Substituent Ratio**					
	CMTKG	BSA	AAM	AA	NPs	MBA	KPS
B3	0.3g	0.3g	0.4g	20 µl	-	0.02g	0.028g
B3NP10	0.3g	0.3g	0.4g	20 µl	10mg	0.02g	0.028g
B3NP20	0.3g	0.3g	0.4g	20 µl	20mg	0.02g	0.028g

3.6. Preparation of drug loaded hydrogel

The 10 ml CFX solution was prepared and the synthesised hydrogel's pellets were then added into the drug solution for 24 h for in vitro drug loading. After 24 h, the pellet was then removed followed by calculation of the amount of unloaded CFX using a calibration curve. UV spectrophotometry was used to find the absorbance of the drug solution at λ_{max} 270 [47].

CHAPTER 4

EXPERIMENTAL SECTIONS

4.1 Swelling Studies

Fabricated hydrogels were tested for swelling in buffer solutions of pH 7.4 and pH 2 .2 for a period of 24 h. The dried hydrogel discs were carefully weighed prior to soaking in the fresh solutions. After 1 hour, each hydrogel disc was removed and excess water was gently blotted off with filter paper and the discs were reweighed. The discs were then returned to the solutions. The procedure was repeated three times to obtain accuracy. The method used to conduct swelling studies was gravimetry method. The purpose of swelling studies was to estimate the impact of added BSA and CuO NPs. The following equation was used to calculate the % ESR.

$$\text{Swelling Ratio } (\%) = \frac{(W_s - W_d)}{W_d} \times 100 \quad (1)$$

W_s = swollen hydrogel's weight

W_d= initial dry weight of the hydrogel

4.2 Sol-gel Content Analysis

The insoluble cross-linked component of hydrogel was identified using sol-gel analysis. A dried hydrogel pellet with a known weight (w_1) was submerged in distilled water for two days in order to extract the soluble portion. The insoluble portion was then stored in an oven at 50°C to achieve a constant weight (w_2). The following formula was used to determine the hydrogels' gel percentage [48].

$$Gel\ Content\ (\%) = \frac{w_2}{w_1} \times 100 \quad (2)$$

4.3 Ciprofloxacin loading and entrapment efficiency

Spectrophotometry was used to measure absorbance at 270 nm in order to calculate the drug concentration in the solution (Da) after 24 hours. Equations (3) and (4) were used to calculate drug entrapment efficiency and drug loading efficiency, respectively [49], [50].

$$EE\ (\%) = \frac{D_0 - D_a}{D_o} * 100 \quad (3)$$

$$DLE\ (\%) = \frac{D_o - D_a}{w_a} \quad (4)$$

where w_a is the weight of the hydrogel pellet submerged in the drug solution and D_o is the theoretical amount of drug.

4.4 In vitro Ciprofloxacin release

In vitro study of the CFX-loaded hydrogel was carried out at two distinct physiological buffers, 2.2 and 7.4. These specific buffers were used to simulate the pH of the stomach and the intestine, respectively, in order to study the release of CFX from hydrogels. A drug-loaded hydrogel pellet of known weight was submerged in 200 ml of the buffer solutions mentioned above. To maintain a constant bath volume for absorbance measurements, 3 ml of sample was removed at regular intervals and replaced with an equivalent volume of fresh buffer. The experiment was conducted at 37°C. The absorbance of the samples collected at regular intervals was calculated at λ_{max} 270 nm after the proper dilutions. The amount of CFX released was determined using the calibration graph.

4.5 Kinetic modelling of Ciprofloxacin

Drug release mechanisms were ascertained using a variety of mathematical models, including Korsmeyer-Peppas, Higuchi, Zero-order, and First-order models. The model with the regression coefficient (R2) value closest to 1 was considered the best fit after the values were compared.

CHAPTER 5

FABRICATION METHOD AND PROCESS

5.1 UV-Visible Spectroscopy (UV-Vis)

Optical spectroscopy is a physical method used to analyze different kinds of solvents and materials. It uses light in the visible, ultraviolet, and near-infrared spectrums. It is based on the Beer-Lambert law, which asserts that a solution's absorbance is directly correlated with both the path length and the concentration of the absorbing species in the solution.

5.1.1. UV-Vis Spectroscopy Principle: A molecule or an ion will undergo an electronic transition when it absorbs radiation. As a result, when a sample absorbs ultraviolet or visible light, the molecules' electronic states change. Electrons will be promoted from their ground state orbitals to higher energy excited state or anti-bonding orbitals by the light's energy. Three different kinds of ground state orbitals could be at play.

1. σ (Bonding) molecular

2. π (Bonding) molecular orbital

3. n (non-Bonding) atomic orbital.

Furthermore, the transition may involve two types of anti-bonding orbitals:

i. σ* orbital.
ii. π* orbital.

n* anti-bonding orbitals do not exist because n electrons do not form bonds. Thus, absorption of ultraviolet and visible light may cause the following electronic transitions [51].

- σ to σ*
- n to σ*
- n to π*
- . π to π*

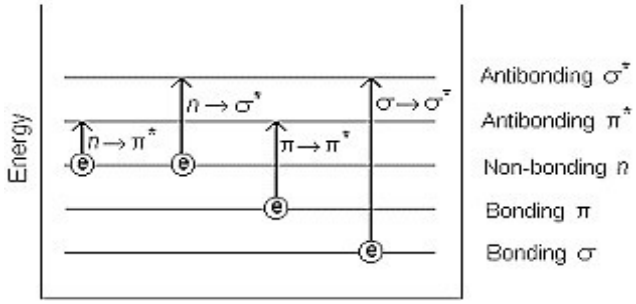

Fig 5.1 Possible Electronic Transitions

5.1.2 Beer Lambert's Law

The absorbance of light by a solution of an absorbing substance is proportional to the concentration of the absorbing substance and the path length, according to the Beer-Lambert law, also called the Bouguer-Beer law.

$$Log\ \frac{I}{I^{\circ}} = A = \varepsilon cl \qquad (4)$$

I° = intensity of the incident radiation
I = intensity of the attenuated radiation
A= absorbance
C= concentration
l= path length
ε= molar extinction coefficient [52].

5.1.3 Instrumentation:

a. **Single beam UV-Vis spectrophotometer**- To analyse one wavelength at a time, the single beam instrument (Fig 5.2) places a filter or monochromator between the source and the sample. Only one beam goes through the sample compartment, and the user has to take measurements of the light intensity (reflected from the reference) before and after the sample is placed in the sample compartment.

b. Double beam UV-Vis spectrophotometer- In the double beam spectrophotometer, one beam passes through the sample while another beam through the reference. A researcher can simultaneously measure the reference standard and the sample [53].

Components of the instrument:

1. Light source
2. Monochromator
3. Sample cell
4. Detector

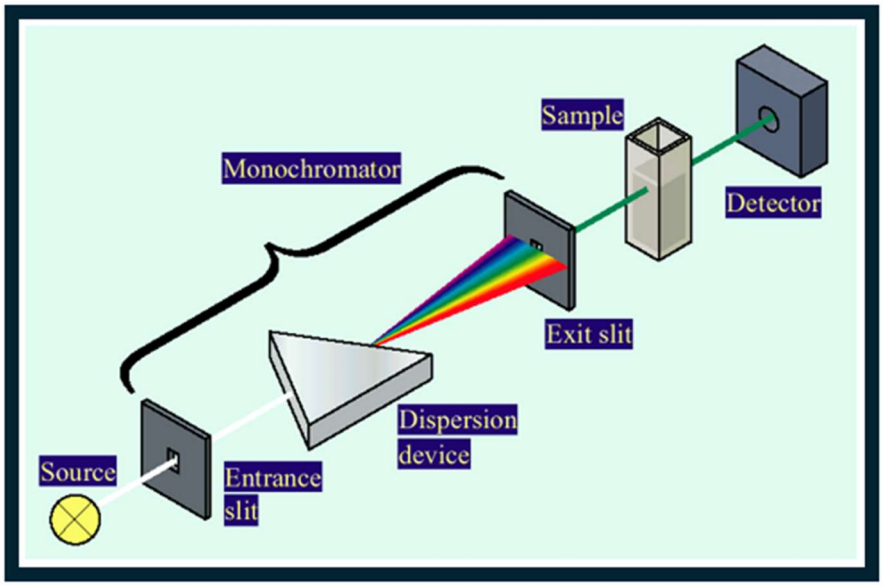

Fig 5.2 Single Beam UV-Vis spectrophotometer

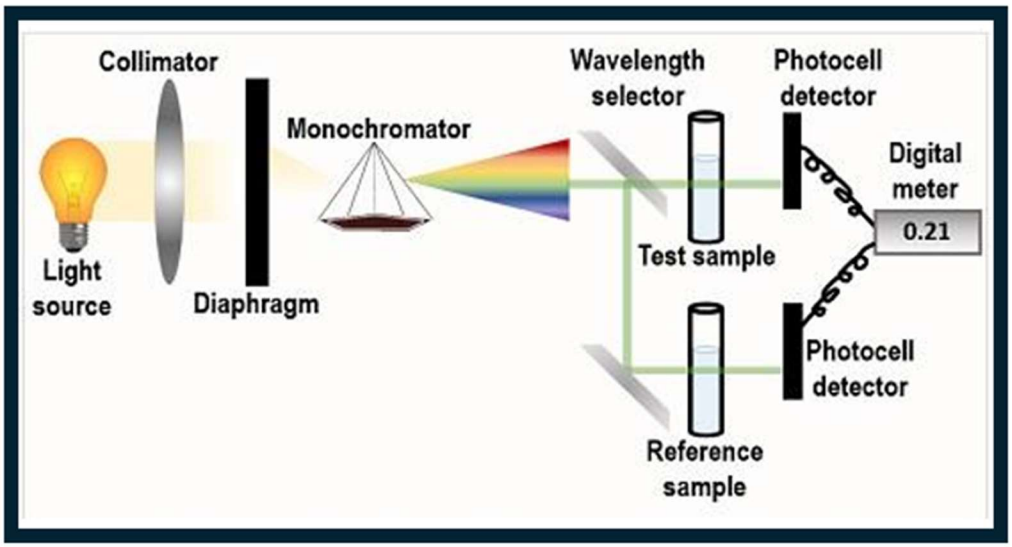

Fig 5.3 Double Beam UV-Vis spectrophotometer

5.2 Attenuated Total Reflection-Fourier Transform Infrared Spectroscopy (ATR-FTIR)

Functional groups, chemical bond and molecular structure of inorganic and organic compound is determined by Fourier transform infrared spectroscopy. FTIR principle works on the following process:

5.2.1 Principle of FTIR

Modern IR spectroscopic instruments frequently employ the FTIR design in order to expedite

the scanning and data collection process. The Michelson interferometer is the fundamental part of the FTIR spectrometer. Fig. 5.4 shows the ATR-FTIR spectrometer's detailed optical layout as well as the methods used to generate the IR spectrum. This apparatus creates the path difference in the infrared beams (emitted from an infrared light source) using a central beam splitter, two stationary and motorized optical mirrors, and an effective detector system. The most popular infrared source for producing infrared beams in FTIR instruments is silicon carbide rod, sometimes referred to as a globar source.The beam splitter divides the infrared beam from the source and directs it toward the motorized and stationary mirrors. Think about the beam that the motorized moving mirror reflects.

It introduces the path difference between this beam and the second beam (from the stationary mirror). These infrared beams have varying path lengths and are susceptible to both constructive and destructive interference. A DTGS (deuterated triglycine sulfate) detector gathers the output as a Fourier transform spectra of the sample response after this recombined infrared radiation interacts with the sample assembly [54].

5.2.2 Instrumentation

FTIR spectrometer is made up of several components:

a. broadband IR source
b. sample compartment
c. Interferometer
d. Detector.

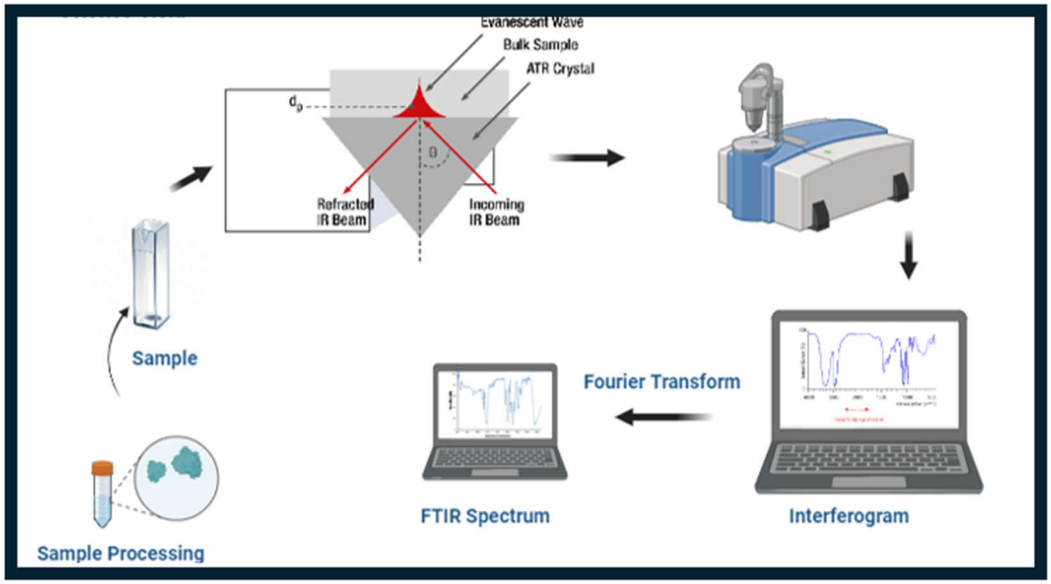

Fig 5.4 FTIR Spectrophotometer

5.3 Field Emission Electron Microscopy (FESEM)

Field emission scanning electron microscopy (FE-SEM), a cutting-edge technique, was used to capture the microstructure image of the materials. Since gas molecules scatter the primary beam and the secondary electrons emitted by the surface under investigation to disrupt the imaging beam, it is generally required to perform FE-SEM in a high-vacuum environment. Particulate materials general shape, surface roughness, structure, and chemistry can all be more accurately described using FESEM [55].

5.3.1. Principle:

The electron beam, after being focused by electromagnetic lenses, is scanned and reflected by the surface of the specimen and the reflected electrons (or interact with the specimen) form an image of the sample surface and topography [56].

5.3.2. Instrumentation:

The FESEM uses-

a) **Field emission gun**- It produces highly concentrated high and low energy electron beams that significantly enhance spatial resolution and allow work to be done at very low potentials (0.02-5 kv). This helps to prevent damage to electron beam-sensitive samples and minimize the charging effect on non-conductive specimens.

b) **In-lens detectors**- These detectors are necessary to get the best results from the equipment because they are made to function at very low acceleration potential and high resolution [57]**.**

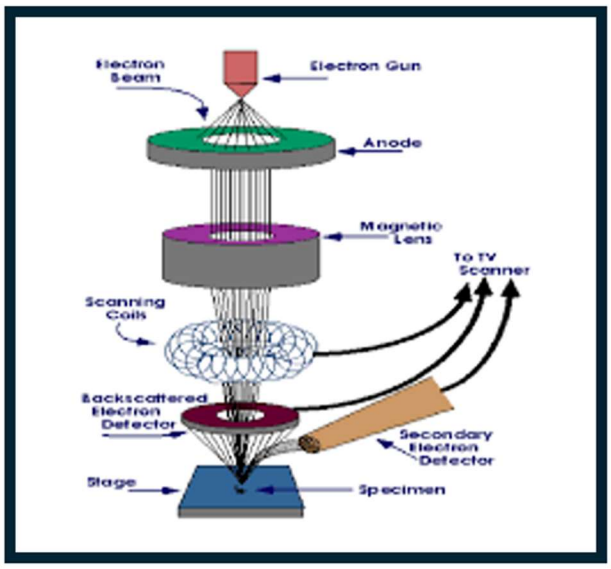

Fig 5.5 Schematic representation of FESEM

5.4 Powder X-Ray Diffraction (PXRD)

Determine the crystal phases, lattice plane spacing, size of crystal existence, preferred orientation, and epitaxial growth of the crystallites in order to examine the crystal content. A database of diffraction patterns can be used to identify materials and compounds because each material has a distinct diffraction pattern.

5.4.1. Principle:

The second one (reflection) is more usual. When the conditions are met which allow the X-ray beam to interfere, the interaction between sample and the X-ray beam creates intense reflected X-rays as a result of constructive interference following Bragg's law [58].

Bragg's Law-

$$n\lambda = 2d\sin\theta \quad (5)$$

n=integer
λ=wavelength
d= interplanar spacing.

5.4.2. Instrumentation:

A high resolution Bruker D8 diffractor was used to study the crystalline phases present of the sample using a Cukα radiation (λ=1.5406 0A) between 2θ range of 10-700C.

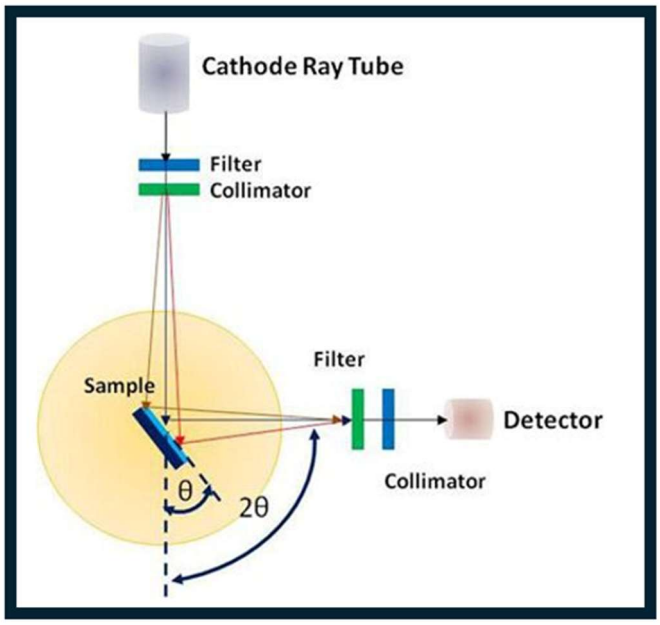

Fig 5.6 Schematic representation Powder X-Ray Diffraction

CHAPTER 6

CHARACTERIZATION TECHNIQUES

6.1 ATR-FTIR Spectroscopy

The ATR-FTIR spectra of CMTKG, AAM, BSA, CuO NPs, composite hydrogel and Nanocomposite hydrogel is Fig 6.1. In CMTKG, the broad band observed at 3300 cm^{-1} due to -OH stretching vibration. The peak at 1600 cm^{-1} observed due to asymmetric vibration of COO^- moiety [59]. The spectrum of AAM indicated the presence of NH_2 group in amide and carbonyl functional groups indicated by the peaks observed at 3345 cm^{-1} and 1668 cm^{-1} respectively [60]. The sharp peak at 1425 cm^{-1} indicates the presence of vinyl group. The BSA spectrum shows three characteristic bands: (i) the sharp Amide I band at 1646 cm^{-1}, indicates the presence of carbonyl group; (ii) the Amide II band at 1525 cm^{-1}, shows the combination of N-H bending and C-H stretching in secondary amide groups; (iii) the Amide III band at 1425 cm^{-1} [61]. The FTIR spectrum of B0 hydrogel, peak at 3300 cm^{-1} is broaden due to Hydrogen bonding. This can also be explained on the basis of participation of the participation of -OH in radical polymerization.

The FTIR spectrum of lysine-coated CuO NPs shows the evident fingerprint of the monoclinic CuO phase. The twin peaks at 553 cm^{-1} (Cu–O stretch) and 671 cm^{-1} (Cu–O bend), confirm the formation of CuO nanoparticles [62]. 3450 cm^{-1} (–NH_2/–OH), 2150 cm^{-1} (lysine amine coordination with Cu^{2+}), and 1010 cm^{-1} (C–N/Cu–O–C interfacial bonding) are indicators of lysine coating. [63]. Together, these peaks demonstrate that lysine's amino and carboxylate groups chemically anchor it to the CuO nanoparticle surface rather than just being physically adsorbed.

The FTIR spectrum of B3 shows the incorporation of BSA in the hydrogel matrix. The strongest evidence of BSA incorporation is the Amide I (1646 cm^{-1}) and Amide II (1525 cm^{-1}) peaks in B3, which are either entirely absent or noticeably different in B0. These peaks function as the molecular fingerprint of BSA's peptide bonds that have been successfully integrated within the hydrogel network because B0 lacks BSA and these peaks only show up in B3. Extensive hydrogen bonding between BSA protein chains and the hydrogel matrix is further confirmed by the broadening of the 3296 cm^{-1} band. The shift of the amide I band as compared to B0 along with some changes in hydroxyl and carboxylate regions suggests the enhanced hydrogen bonding and electrostatic interactions between BSA and grafted poly(AAM-co-AA). This confirms the formation of stable and interconnected CMTKG-g-poly(AAM-co-AA)/BSA hydrogel network.

The FTIR spectrum of nanocomposite hydrogel show absorption band at 1214 cm^{-1}, attributed

to C-N stretching vibrations of amide groups from BSA and polyacrylamide and contribution of lysine amino groups, coating the CuO NPs. The band at 588 cm^{-1}, which is the shifted Cu–O stretching vibration (from 553 cm^{-1} in pure CuO NPs), is the conclusive peak verifying CuO NP incorporation in B3NP20.Its presence in B3NP20, which is not present in bare B3 hydrogel, clearly indicates that the nanoparticle loading was successful. The band at 671 cm^{-1} in CuO NPs is merged in B3NP20 spectrum which indicates the its interaction with polymer matrix. Further evidence of the physicochemical interaction between the NPs and the hydrogel matrix is provided by the corresponding changes in the amide and hydroxyl bands.

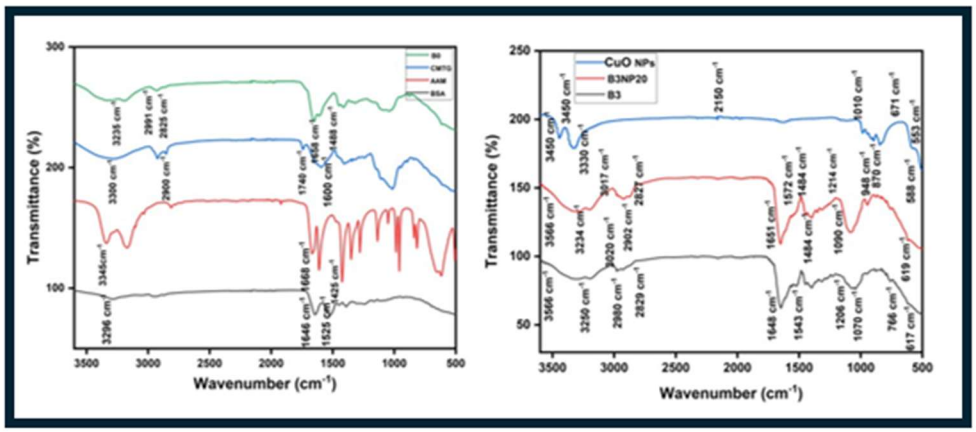

Fig 6.1 FTIR Spectra of a) B0, CMTKG, AAM, BSA b) Lysine-coated CuO nanoparticles, Nanocomposite hydrogel (B3NP10), Composite hydrogel (B3)

6.2 PXRD

The Debye-Scherrer equation was utilized to estimate the crystalline size of 26.23±2.95 nm for CuO NPs. The PXRD pattern of the lysine-coated CuO nanoparticles shows several intense and sharp diffraction peaks, pointing the crystalline nature of the prepared CuO nanoparticles. The prominent peaks observed at 2θ of around 35°, 38°, 48°, 58°, 61°, 66° and 68° are of the characteristic monoclinic phase of CuO, which is the desired phase of the product. The fact that the crystallite size is less than 100 nm indicates that the biosynthesized CuO NPs are nanocrystalline [64]. This confirms that the synthesized nanoparticles possess a monoclinic structure and consist of a single-phase CuO [65].

By contrast, the nanocomposite hydrogel presents a broad diffuse hump with low peak intensity, suggesting the presence of mainly amorphous polymeric hydrogel matrix [46] The diffraction peak intensity and peak width of CuO decreased, indicating successful dispersion and encapsulation of CuO nanoparticles into the crosslinked polymer network without changing the crystal structure of CuO, because the crystal structure of CuO remained the same

even after the incorporation of CuO nanoparticles into the hydrogel. This indicates that the nanocomposite hydrogel is stable and has good compatibility between the polymer matrix and embedded CuO nanoparticles [66].

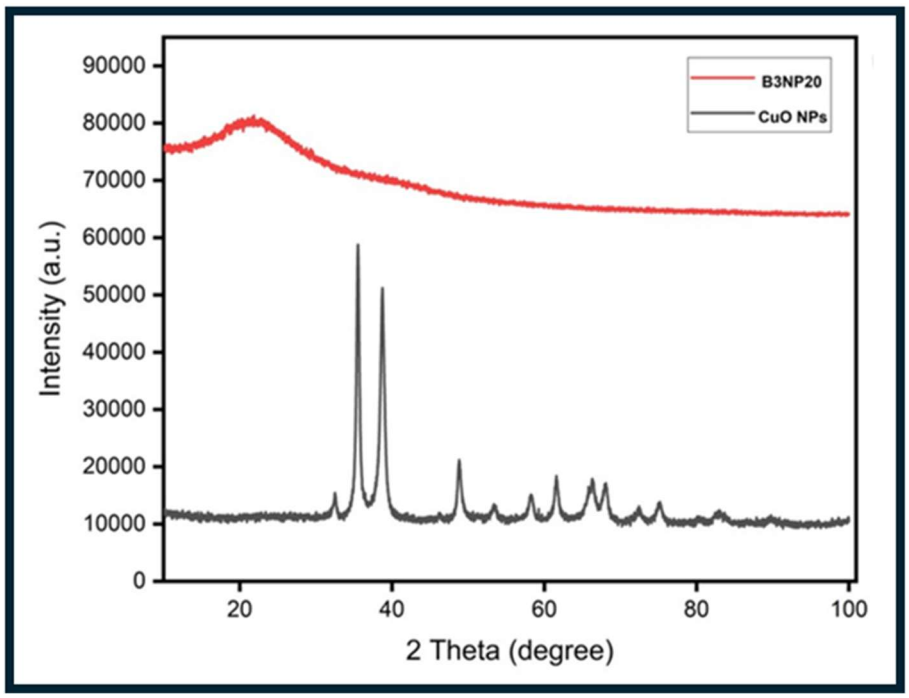

Fig 6.2 PXRD pattern of CuO nanoparticles and nanocomposite hydrogel.

6.3 FESEM

FESEM image of the CuO NPs, composite hydrogel and nanocomposite hydrogel are displayed in fig 6.3. The lysine coated CuO nanoparticles have rod and flake-like shape as shown in the image. It is seen that these flaky shaped morphology arised due to assembly of rods shaped particles [67]. The nanoparticles appear to be clustered together, forming a porous and interconnected network. The elongated structures (with sharp edges and rough surfaces) are observed, showing good crystallinity of the CuO nanoparticles. Surface morphology shows high aggregation of the nanoparticles which is common with the metal oxide nanoparticles synthesized biologically because of intermolecular interactions and high surface energy. The lysine coating play a role a stabilizing and capping agent and participates in the process of forming the nanoscale structure [68].

The composite hydrogel reveals the continuous, uniform and homogeneous surface, suggesting that the CMTKG, BSA and PAM has blended successfully and cross linked together in the hydrogel matrix [69] . A number of micropores and voids can be seen scattered with the surface in small circular dark areas. The presence of pores represents a medium porosity.

The Bio-nanocomposite hydrogel shows a surface with compact, rough and heterogeneous, closely connected ridge-like and granular features. The pore size and surface roughness and surface roughness of the hydrogels have increased with the addition of the CuO nanoparticles suggesting strong interactions between the polymeric matrix and nanoparticles. This suggests the ability of CuO nanoparticles to function as cross-linkers [70] . The surface is wrinkled and aggregated, and uniformly distributed domains of nanoparticles can be seen, which is an indication of a successful embedding of the CuO nanoparticle in the hydrogel network [69].

The high density and texture of this architecture indicate better structural strength, higher surface area and possible use for biomedical applications like drug delivery systems. Thus, facilitate the effective encapsulation of CFX within the polymer matrix.

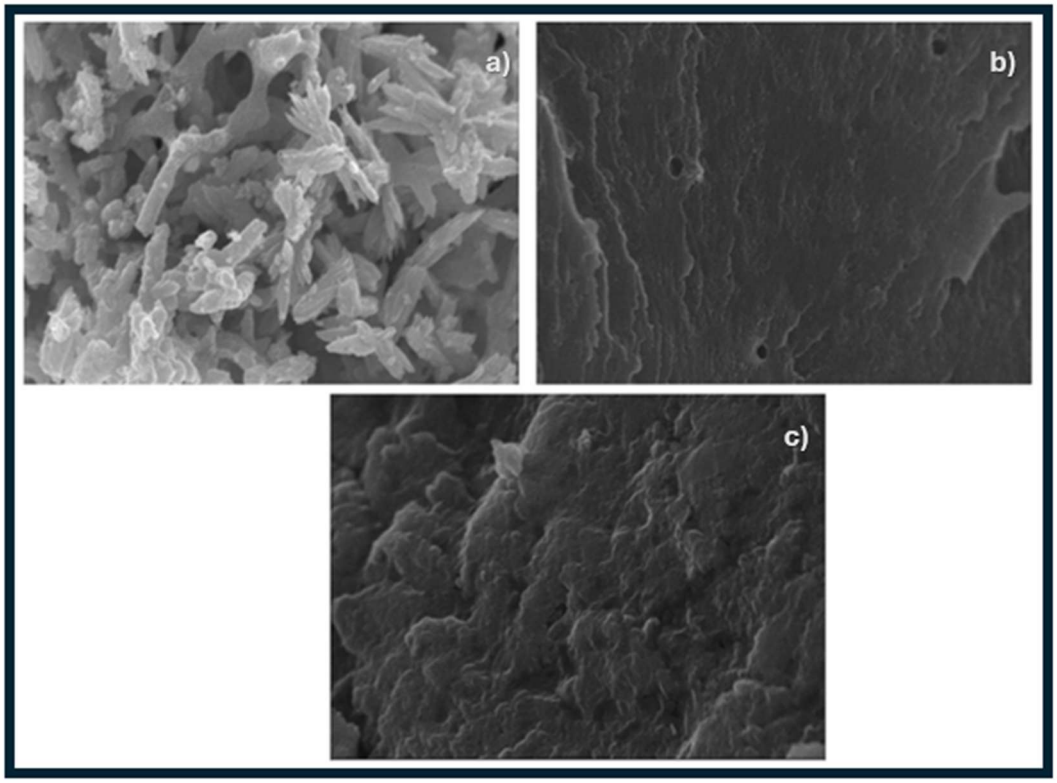

Fig 6.3 FESEM images at 30 KX magnification of (a) CuO NPs (b) Composite hydrogel (c) Nanocomposite hydrogel.

6.4 Cytocompatibility tests

6.4.1 MTT Assay

The cytocompatibility was checked by MTT assay using L929 Fibroblast. The data of the CFX-loaded nanoparticle composite hydrogel exhibits highly cytocompatible nature for the cells used in the study. The nanocomposite CFX-loaded hydrogel showed low cytotoxicity with cell viability over 90% even at the higher concentrations from 50 to 250 µg. The viability values, however, are still above the accepted biocompatibility threshold which confirm the non-toxicity and bio-safety of the nanocomposite hydrogel. It is considered that a material with more than 75% of cell viability is non-cytotoxic [71].

Based on the results from these tests, the CFX-loaded nanocomposite hydrogel is found to be biocompatible and can be used in biomedical and drug delivery applications.

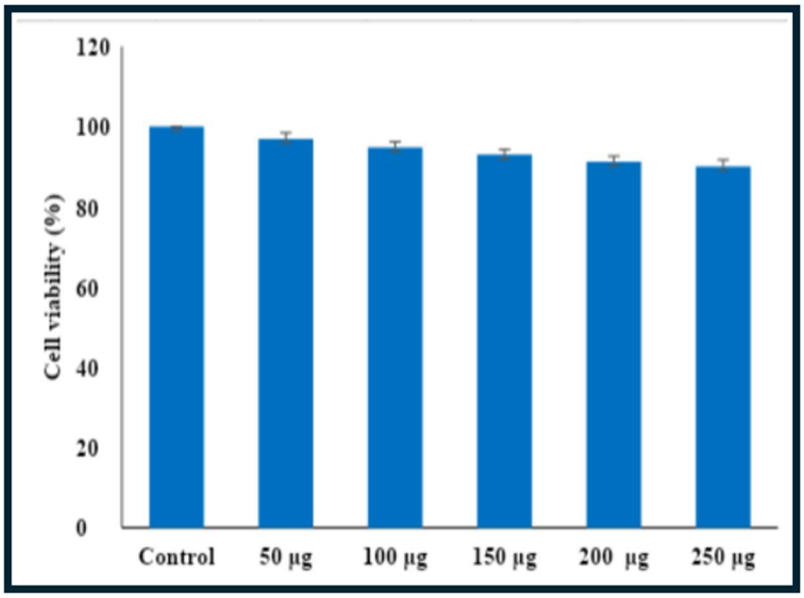

Fig 6.4.1 MTT Assay showing cell viability

6.4.2. Antibacterial Studies

The results of the sample's antibacterial activity against various microbes using the disc diffusion method [72]. At a concentration of 100 µg/ml, the bare nanocomposite hydrogel sample showed inhibitory activity against Escherichia coli (9 mm) and Staphylococcus aureus (10 mm) at a concentration 100 µg/ml [73].

At 80 µg/ml concentration, the sample exhibited the antibacterial activity against all the tested bacteria, but it was more susceptible against Staphylococcus aureus (9 mm) [68].

The CFX-loaded nanocomposite hydrogel sample demonstrated inhibitory activity against Escherichia coli (10 mm) and Staphylococcus aureus (11 mm). The sample demonstrated antibacterial activity against all tested bacteria at a concentration of 80 µg/ml, but it was somewhat more vulnerable to Staphylococcus aureus (10 mm) [68]. The sample's inhibitory effects on all of the strains used in this investigation increased as its concentration rose from 60 to 80 µg/ml. Thus, the CFX-loaded hydrogels showed considerable growth inhibition zones. This observation confirmed the release of ciprofloxacin from hydrogels [74].

Samples	**Concentrations (µg/ml)**	**Organisms/Zone of inhibition (mm)**	
		Staphylococcus aureus	***Escherichia coli***
Samples	60	7	6
	80	9	7
	100	10	9
Standard (Std) (Amoxicillin)	10 µl/disc	13	11
DMSO	10 µl/disc	0	0

Fig 6.4.2a Antibacterial Activity of bare nanocomposite hydrogel.

Samples	**Concentrations (µg/ml)**	**Organisms/Zone of inhibition (mm)**	
		Staphylococcus aureus	***Escherichia coli***
Samples	60	9	8
	80	10	9
	100	11	10
Standard (Std) (Amoxicillin)	10 µl/disc	12	13
DMSO	10 µl/disc	0	0

Fig 6.4.2b Antibacterial activity of CFX-loaded nanocomposite hydrogel.

6.5 Zeta Potential

Using Dynamic Light Scattering (DLS), the zeta potential of the CuO NPs coated with lysine is displayed in Fig. 6.5. The stability of the produced CuO NPs is indicated by the zeta potential, which was found to be –23 mV. According to reports, the nanoparticles zeta potential is more stable when it is closer to −30 mV [75].

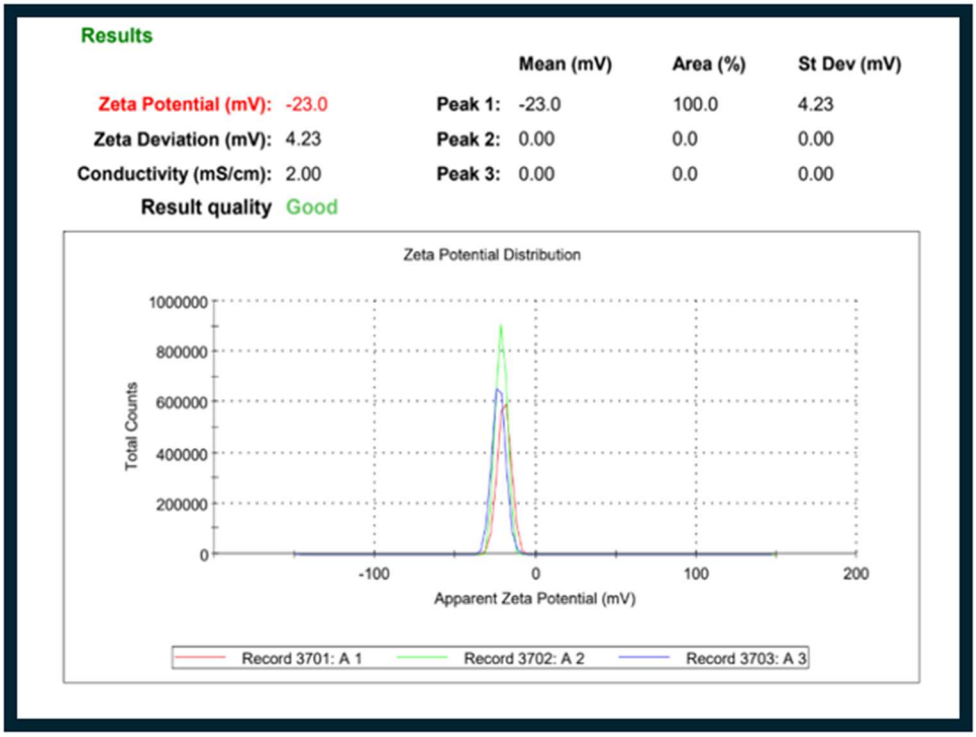

Fig 6.5 Zeta Potential of CuO nanoparticles.

CHAPTER 7

RESULT AND DISCUSSION

7.1 Overview of CMTKG-g-poly(AAM-co-AA)/BSA/CuO nanocomposite hydrogel and CFX- loaded CMTKG-g-poly(AAM-co-AA)/BSA/CuO nanocomposite hydrogel

Developed hydrogel network is composed of carboxymethyl tamarind kernel gum (CMTKG), bovine serum albumin (BSA), acrylamide (AM), acrylic acid (AA) and lysine-coated copper oxide (CuO) nanoparticles. KPS was used as a free-radical initiator for the preparation of hydrogels. Thermal decomposition of KPS produces sulfate radical anions, which are able to initiate the polymerization of the acrylamide and acrylic acid monomers. The monomers undergo attack by these radicals to produce an increase in the length of growing polymer chains. This helps to graft the monomers onto the CMTKG backbone. N,N′-Methylenebisacrylamide (MBA) was used as the chemical crosslinking agent. MBA has two polymerizable vinyl groups which are involved in free-radical polymerization reaction [76]. When forming the network, each vinyl group will bind to different growing polymer chains, which will form covalent bonds between the polyacrylamide chains and the poly(acrylic acid) chains. These interactions provide network stabilization and increase the mechanical strength of the hydrogel network [77].

Chemically crosslinked CMTKG-g-poly(AAM-co-AA)/BSA/CuO) network is formed as a result of the combination of KPS and MBA. The bovine serum albumin and lysine-coated CuO nanoparticles then enter into the hydrogel matrix through hydrogen bonding, electrostatic interactions.

The bovine serum albumin (BSA) is a multifunctional bioactive component inside the hydrogel. The amino acid residues of BSA contain amino ($-NH_2$), carboxyl (-COOH) groups. The carboxyl group of BSA crosslinked with the vinyl group of AAM. These interactions help in the incorporation of BSA into the polymeric network and in enhancing the biocompatibility of the hydrogel.

The addition of lysine-coated CuO nanoparticles further strengthens the hydrogel structure. The molecules of lysine are bound to the surface of CuO, leaving amino and carboxyl functional groups to the polymer matrix [78]. Lysine's carboxylate groups bind to the surface copper ions, creating a stable coating around the nanoparticles.

Ciprofloxacin was incorporated in the CMTKG-g-poly(AM-co-AA)/BSA/CuO nanocomposite hydrogel by hydrogen bonding, electrostatic interaction [79]. The collective

interactions resulted in an efficient drug encapsulation and sustained drug release behaviour.

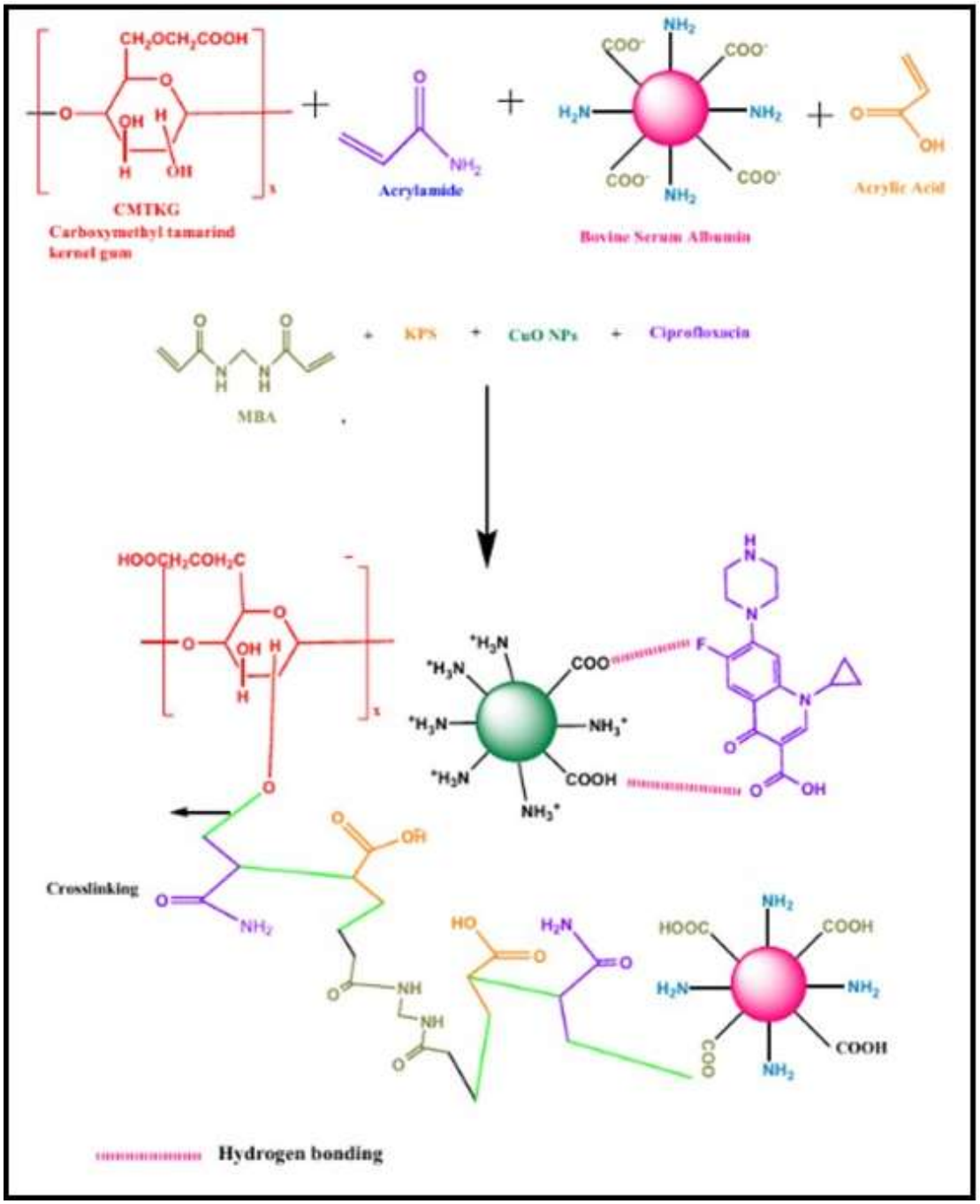

Fig 7.1 Proposed mechanism of CFX-loaded CMTKG-g-poly(AAM-co-AA)/BSA/CuO nanocomposite hydrogel.

7.2 Swelling Studies

All the synthesized hydrogels were subjected to swelling analysis in both pH 7.4 and pH 2.2. It was found that there was a significant increase in swelling at pH 7.4 as compared to swelling at pH 2.2. The three major factors that are usually responsible for the swelling of hydrogels are

(i) the creation of inter-molecular voids inside the three-dimensional (3-D) network structure (ii) the porosity of the hydrogel surface (iii) the presence of hydrophilic moiety in the hydrogel matrix.[80]. The anionic carboxylate groups are abundantly present in the overall hydrogel network as these are present in CMTKG and Acrylic acid. The main reasons for the higher swelling of the corresponding hydrogels at ph 7.4 were the presence of hydroxyl groups that are hydrophilic and the electrostatic interaction force of the anionic carboxylate groups, and the osmotic pressure generated inside the hydrogels by the presence of the anionic carboxylate groups These physical interactions may increase the number of crosslinking points, which would raise the crosslink density and in turn, decrease the hydrogel's pores size for water absorption [74].

7.2.1 Impact of BSA

The BSA concentration had a significant impact on the hydrogels' swelling (Fig. 6.2). Table 1 illustrates that the synthesized hydrogel (B0) without BSA and NPs exhibits greater swelling than all other samples. As the BSA concentration increased (from 0g to 0.3g), the swelling capacity decreased because the polymeric network's free volume decreased as physical interactions increased, increasing the cross-linking density. Thus, increasing the BSA concentration resulted in a significant reduction in swelling at both pH 7.4 and pH 2.2 [81].

7.2.2. Impact of CuO NPs

While varying concentrations of NPs (10–20 mg) are investigated for swelling, the concentration of BSA is maintained at 0.3 g. The swelling ratio initially decreases with an increase in NPs content up to a maximum of 20 mg. However, as the hydrogel network's cross-linking increased. Consequently, the swelling is reduced on increasing NPs amount. This may be explained by CuONP's knot-tying functions. The chelation of certain hydroxyl and amine groups in the hydrogel networks with CuO nanoparticles may be the cause of CuONPs' knot-tying ability [82]. CuO NPs are cytotoxic and it was found that cell viability is concentration dependent with CuO NPs [83].

The surface charge of CuO nanoparticles is negative and the surface charge of Lysine is positive with amine charge, prefers to bind to the surface of CuO nanoparticles in preference to its carboxyl groups [84]. Hence, the positive amino acid coating to the NPs which increased their stability, was achieved by adding Lysine [45].

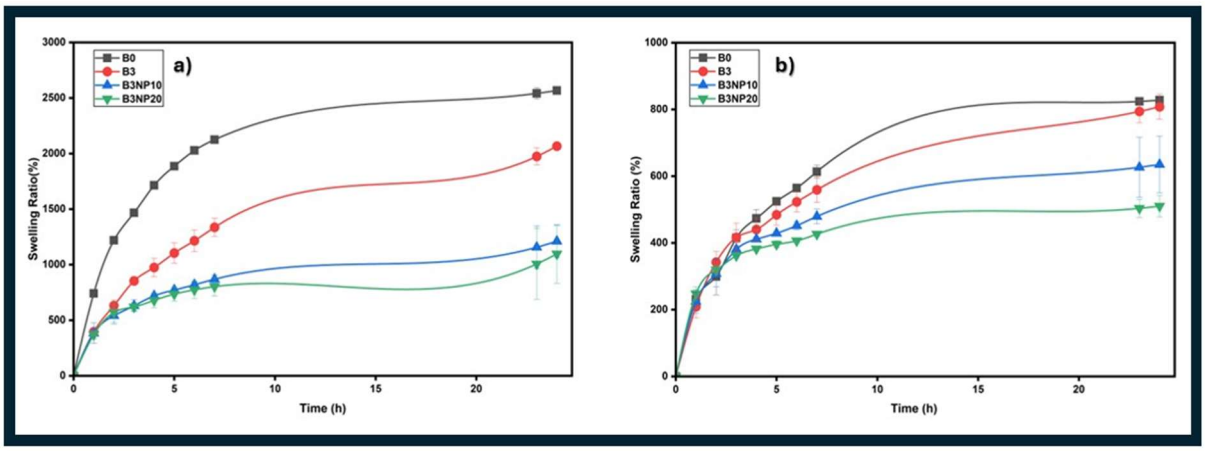

Fig 7.2 a) Swelling Ratio of B0, B3, B3NP10, B3NP20 at 7.4 pH b) Swelling Ratio of B0, B3, B3NP10, B3NP20 at 2.2 pH.

The above Fig 6.2 shows the effect of concentration of both BSA and NPs on the ESR % of the hydrogels.

7.3 Loading of Drug and Encapsulation Efficiency

The drug loading and drug encapsulation efficiency of the CFX loaded composite and CFX-loaded nanocomposite hydrogel was studied. The DEE (%) and DLE (%) is shown in table mentioned below.

Table 3

Hydrogel Composition	Drug entrapement efficiency (%)	Drug Loading efficiency (%)
B0	37	7.7
B3	42	9.6
B3NP10	51.5	10.8
B3NP20	54.4	11.5

7.4 In vitro release of CFX

The in vitro investigation was performed on CFX loaded nanocomposite hydrogel as shown in Fig. 6.4. This observation suggests that the release of the drug from the drug loaded nanocomposite hydrogel is pH dependent. Considerable amount of release of the drug was seen at pH 2.2 when compared with the release at pH 7.4. Nanocomposite hydrogel shows drug release 59-62% in 2.2 pH and 40-50.5% in 7.4 pH in 7h. In B0 hydrogel which is devoid of both BSA and NPs, showed burst drug release of 98% in both acidic and alkaline pH. Hydrogels swell more in basic media, but the drug release percentage is higher in acidic media. The solubility behaviour of CFX with respect to pH, which decreases in the pH range of 2.2 to 7.4

and increases in acidic pH. This can account for the higher release percentage of the model drug [85]. The addition of BSA resulted in decreased drug release. The nanocomposite hydrogel showed comparatively minimum drug release. This is due to the increased cross-linking in hydrogel network. Thus, the incorporation of BSA and NPs resulted in more controlled and sustained drug release.

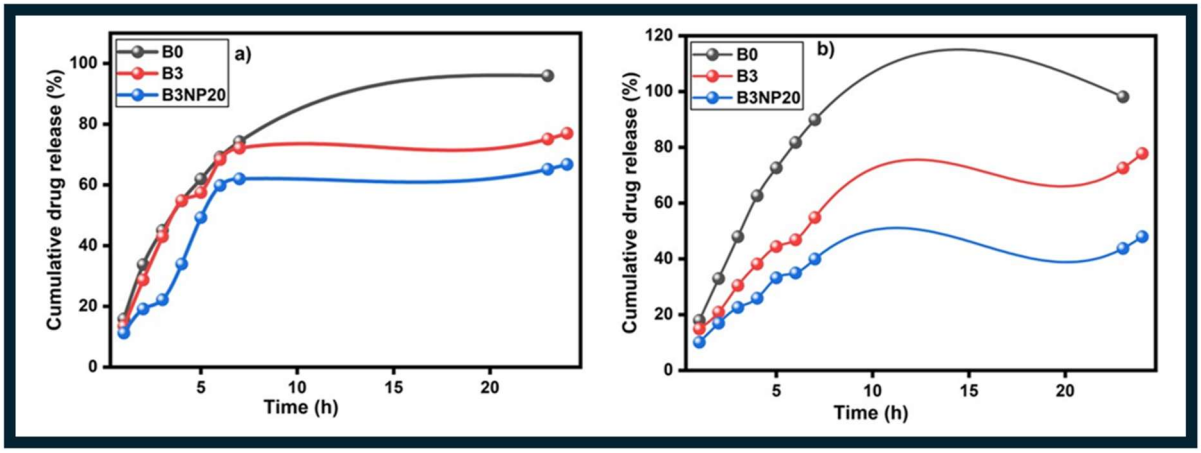

Fig 7.4 a) Drug Release of B0, B3, B3NP10, B3NP20 at pH 2.2 b) Drug Release of B0, B3, B3NP10, B3NP20 at pH 7.4.

The above fig 7.4 shows the effect of the concentration of both BSA and NPs on the drug release from the hydrogels.

7.5 In vitro Antibacterial activity against E. coli and S. aureus

The nanocomposite hydrogel sample showed inhibitory activity against *Escherichia coli* (9 mm) and *Staphylococcus aureus* (10 mm) at a concentration 100 µg/ml. The CFX-loaded nanocomposite hydrogel sample showed inhibitory activity against *Escherichia coli* (10 mm) and *Staphylococcus aureus* (11 mm) at the same concentration as of above. The sample demonstrated antibacterial activity against all tested bacteria at a concentration of 80 µg/ml, but it was somewhat more vulnerable to *Staphylococcus aureus* in both cases [68]. i.e. 9 mm for nanocomposite hydrogel and 10 mm for CFX-loaded bio-nanocomposite hydrogel. Patients with osteomyelitis typically had S. aureus and E. coli. In this context, the ciprofloxacin-loaded nanocomposite hydrogels, antibacterial properties against Gram-positive *S. aureus* and Gram-negative *E. coli* bacteria were slightly more susceptible to antibacterial activity from the bare nanocomposite hydrogels. The hydrogels loaded with CFX displayed significant growth inhibition zones. The release of ciprofloxacin from hydrogels was confirmed by this observation. The results showed that the hydrogels loaded with CFX may be a promising

treatment option for osteomyelitis [74].

Fig 7.5 Showing Antimicrobial activity against S. aureus and E. coli by a) Nanocomposite Hydrogel b) CFX-loaded nanocomposite Hydrogel.

7.6 Kinetic Modelling of Ciprofloxacin

The drug release behaviour of CFX-loaded hydrogel formulations (B0, B3, B3NP10 and B3NP20) was analyzed by applying the kinetic models of Zero-order, First-order, Korsmeyer–Peppas and Higuchi at pH 7.4 and pH 2.2 (Table 4). The coefficient of determination (R^2) values suggest that there were medium pH and hydrogel composition differences in the release mechanism. The First-order model had the highest value of R^2 for B0 ($R^2 = 0.842$) and B3 ($R^2 = 0.953$) indicating that the release of drug from formulations was concentration-dependent, with a decrease in the drug amount released as the amount of drug remaining in the matrix decreased. The best fit was obtained with the B3NP10 formulation, which was fitted to Higuchi model with an R^2 value of 0.948, suggesting that the release of CFX was mostly controlled by diffusion through the swollen hydrogel matrix. Likewise, the fitting of B3NP20 model for Higuchi ($R^2 = 0.812$) and Korsmeyer–Peppas ($R^2 = 0.869$) models suggested diffusion and polymer relaxation mechanism both. The Korsmeyer–Peppas release exponent (n) values varied from 0.452 to 0.9, suggesting that the release mechanism evolved from Fickian diffusion, to Non-Fickian transport, as a function of the concentration of nanoparticles and the network structure. The nanocomposite hydrogel (B3NP20) obeys Non-fickian diffusion [85]. The same formulation follows Fickian diffusion mechanism at pH 7.4 since n= 0.452 i.e. $n \leq 0.5$ [86].

The highest R^2 values (0.953 to 0.981) and best fits of the release data were achieved using the Korsmeyer–Peppas model for all formulations at pH 2.2. The release exponent (n) values were 0.760-0.935, which is higher than the known 0.45 and mostly in the range of non-Fickian

transport. This indicates that the drug release under acidic condition was the regulated by the drug diffusion along with polymer chain relaxation [87].

The presence of lysine-coated CuO nanoparticles changed the release kinetics because of the added complexity of the matrix and the presence of other interactions between the polymeric network, the nanoparticles and ciprofloxacin. In particular, the B3NP10 formulation showed a diffusion controlled behaviour at physiological pH, while the higher NPs loading B3NP20 formulation favoured the mixed transport mechanisms. The overall kinetic analysis indicates that the drug release process from the developed nanocomposite hydrogels is strongly pH dependent: concentration dependent and diffusion controlled release dominate at pH 7.4 while an anomalous transport mechanism dominates at pH 2.2. The results of this study prove the feasibility of delivering the antibiotic CFX at the desired rate and in response to specific triggers using the nanocomposite hydrogel system.

Table 4 Different Kinetic models used for Drug release analysis.

Model	**Equations**	**Reference**
Zero Order	$W_t = W_\infty + k_0 t$ k_0 = zero-order constant	[88]
Higuchi	$W_t/W_\infty = k_{HG} t^{1/2}$ k_{HG} = Higuchi constant	[38]
First Order	$\text{Log } W_t = \text{Log } W_\infty + \frac{kt}{2.303}$ k = first order constant	[89]
Korsmeyer–Peppas	$W_t/W_\infty = kt^n$ k = kinetic constant n = diffusion exponent	[90]

Table 5 Kinetic modelling data of **CFX-**loaded nanocomposite hydrogel at pH 7.4 and 2.2.

Hydrogel Formulation	**Zero Order**		**First Order**		**Korsmeyer peppas**		**Higuchi**	
	pH 7.4	**pH 2.2**	**pH 7.4**	**pH 2.2**	**pH 7.4**	**pH 2.2**	**pH 7.4**	**pH 2.2**
	R^2	**R^2**	**R^2**	**R^2**	**R n**	**R n**	**R^2**	**R^2**
B0	0.529	0.752	0.8420	0.518	0.999 0.9	0.981 0.85	0.723	0.878
B3	0.838	0.509	0.9528	0.367	0.989 0.686	0.981 0.935	0.934	0.668
B3NP10	0.883	0.664	0.689	0.469	0.924 0.897	0.955 0.76	0.948	0.800
B3NP20	0.676	0.553	0.516	0.453	0.869 0.452	0.953 0.92	0.812	0.695

7.7 Sol-gel Content Analysis

The gel fraction and degree of swelling is dependent on the amount of BSA and nano copper oxide. Addition of BSA and CuO NPs (10 and 20mg) to the CMTKG-g-poly(AAM-co-AA)/BSA hydrogel increased its gel percentage from 76 % for B0 hydrogel, 82 % for B3, 91% for B3NP10 and 92 % for nanocomposite (B3NP20) hydrogel containing 20 mg CuO NPs. A direct relationship between gel percentage and amount of NPs and BSA was evident. The nanoparticles and BSA embedded in the in the hydrogel act as cross-linking points. Thus, enhance the entangled structure and gel density of hydrogels. The higher gel percentage improves the mechanical properties of hydrogels. This is due to the stronger interactions between the polymer chains [91].

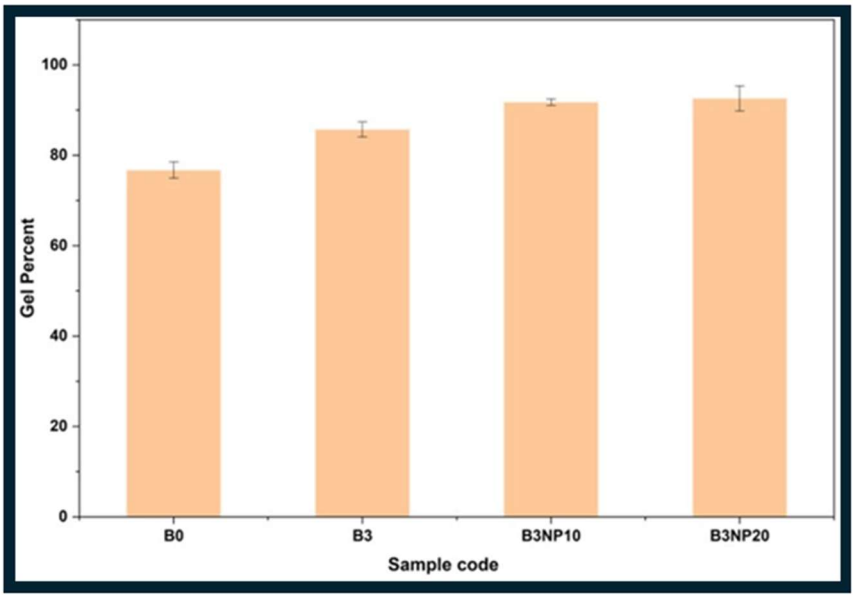

Fig 7.7 Sol-gel Analysis

CHAPTER 8

CONCLUSION

8.1 Conclusion

In the present study, a novel pH-responsive CMTKG-g-poly(AAM-co-AA)/BSA hydrogel loaded with green synthesized CuO nanoparticles that were coated with the lysine was successfully developed and characterized for controlled delivery of the antibiotic ciprofloxacin. The CuO nanoparticles were synthesized by an eco-friendly green synthesis route by using *Catharanthus roseus* (*Madagascar periwinkle*) leaf extract and the hydrogel was synthesized by free radical graft polymerization by using CMTKG, BSA, acrylamide and acrylic acid. The addition of BSA and CuO nanoparticles also enhanced the structural integrity and crosslinking density of the hydrogel network which led to less swelling of the hydrogel and thus prevented burst drug release. Swelling studies showed that the system was highly sensitive to pH and the pH 7.4 showed a high swelling and the acidic pH showed a low swelling thereby making it suitable for pH responsive drug delivery application. The optimized nanocomposite hydrogel demonstrated sustained and controlled release profile of ciprofloxacin, higher drug release at acidic pH. It fits well with the Korsmeyer–Peppas kinetic model. The FTIR, PXRD and FESEM characterization studies validated the formation of the hydrogel, incorporation of CuO nanoparticles and the porous nature essential for the encapsulation and release of drug. The synthesized CuO nanoparticles were crystalline in nature and had a higher surface area and antibacterial activity due to their nanoscale size. Antimicrobial studies showed great inhibition against *E. coli* and *S. aureus*, thus confirming the synergistic antibacterial effect of the combinations of ciprofloxacin and CuO nanoparticles. Moreover, MTT assay indicated the excellent biocompatibility of the prepared hydrogel system with a cell viability of over 90%, an essential requirement for use in biomedical applications. Based on literature analysis of similar drug delivery systems made of hydrogel, it is found that the mechanical strength, drug encapsulation efficiency, antibacterial activity and controlled drug release behaviour of the composite materials are improved with the addition of natural polysaccharides and synthetic polymers and metal oxide nanoparticles. The addition of CMTKG and BSA enhance the hydrophilicity, biodegradability and biocompatibility of conventional PAM-based hydrogels, while the antimicrobial activity and environmentally friendly synthesis process of phytogenic CuO nanoparticles provide an extra benefit.

In summary, the developed CMTKG-g-poly(AAM-co-AA)/BSA/CuO nanocomposite hydrogel exhibited promising ability to function as a controlled release drug delivery system in oral drug delivery, boasting the antibacterial activity as well as excellent cytocompatibility. The study accentuates the potential of the hydrogels prepared by the green synthesis of metal

oxide nanoparticle for advanced applications in biomedical and pharmaceutical field. Further studies can be conducted to evaluate the nanoparticles in vivo, to carry out long-term stability studies and to optimize the concentration of nanoparticles for targeted therapeutic applications.

CHAPTER 9

REFERENCES

References

[1] F. Ullah, M. B. H. Othman, F. Javed, Z. Ahmad, and H. M. Akil, "Classification, processing and application of hydrogels: A review," Dec. 01, 2015, *Elsevier Ltd*. doi: 10.1016/j.msec.2015.07.053.

[2] S. Mitura, A. Sionkowska, and A. Jaiswal, "Biopolymers for hydrogels in cosmetics: review," Jun. 01, 2020, *Springer*. doi: 10.1007/s10856-020-06390-w.

[3] T. C. Ho *et al.*, "Hydrogels: Properties and Applications in Biomedicine," May 01, 2022, *MDPI*. doi: 10.3390/molecules27092902.

[4] S. Priya Nagam, A. Naga Jyothi, J. Poojitha, S. Aruna, and R. Rao Nadendla, "A COMPREHENSIVE REVIEW ON HYDROGELS," 2016.

[5] M.-D. Onofrei and A. Filimon, "Cellulose-based hydrogels: Designing concepts, properties, and perspectives for biomedical and environmental applications."

[6] J. M. Dodda, K. Deshmukh, D. Bezuidenhout, and Y.-C. Yeh, "Hydrogels: Definition, History, Classifications, Formation, Constitutive Characteristics, and Applications." [Online]. Available: www.rsc.org

[7] A. Kumar, S. Pandey, K. Kumar, S. Krishnamoorthi, and K. Tungala, "Hydrogels: classification, cross-linking methods, characteristics, and current trends in biomedical applications," Feb. 01, 2026, *Springer Science and Business Media Deutschland GmbH*. doi: 10.1007/s00289-025-06053-2.

[8] B. S. Kaith, A. Singh, A. K. Sharma, and D. Sud, "Hydrogels: Synthesis, Classification, Properties and Potential Applications—A Brief Review," Dec. 01, 2021, *Springer*. doi: 10.1007/s10924-021-02184-5.

[9] L. Chauhan, P. Thakur, and S. Sharma, "PHARMACEUTICAL SCIENCES HYDROGELS: A REVIEW ON CLASSIFICATION, PREPARATION METHODS, PROPERTIES AND ITS APPLICATIONS," *Hydrogels: A Review On Classification, Preparation Methods, Properties And Its Applications., Indo Am. J. P. Sci*, no. 06, p. 6, 2019, [Online]. Available: http://www.iajps.com

[10] “Glossary of basic terms in polymer science (IUPAC Recommendations 1996).”

[11] N. Zoratto and P. Matricardi, “Semi-IPN- and IPN-based hydrogels,” in *Advances in Experimental Medicine and Biology*, vol. 1059, Springer New York LLC, 2018, pp. 155–188. doi: 10.1007/978-3-319-76735-2_7.

[12] K. Mukherjee *et al.*, “Alginate based semi-IPN and IPN hydrogel for drug delivery and regenerative medicine,” Feb. 01, 2024, *Editions de Sante*. doi: 10.1016/j.jddst.2024.105402.

[13] “semi crystalline, amorphous and crystalline”.

[14] X. Meng, G. Jin, and R. Yang, “A quantum chemical and molecular dynamics simulation study on photo-oxidative aging of polyethylene: Mechanism and differences between crystalline and amorphous phases,” *Polym. Degrad. Stab.*, vol. 217, Nov. 2023, doi: 10.1016/j.polymdegradstab.2023.110536.

[15] S. Venkatram, J. McCollum, N. Stingelin, and B. Brettmann, “A close look at polymer degree of crystallinity versus polymer crystalline quality,” *Polym. Int.*, vol. 72, no. 10, pp. 855–860, Oct. 2023, doi: 10.1002/pi.6508.

[16] M. Polińska, A. Rozanski, A. Galeski, and J. Bojda, “The Modulus of the Amorphous Phase of Semicrystalline Polymers,” *Macromolecules*, vol. 54, no. 19, pp. 9113–9123, Oct. 2021, doi: 10.1021/acs.macromol.1c01576.

[17] M. E. Tuttle, “A BRIEF INTRODUCTION TO POLYMERIC MATERIALS.”

[18] L. Chauhan, P. Thakur, and S. Sharma, “PHARMACEUTICAL SCIENCES HYDROGELS: A REVIEW ON CLASSIFICATION, PREPARATION METHODS, PROPERTIES AND ITS APPLICATIONS,” *Hydrogels: A Review On Classification, Preparation Methods, Properties And Its Applications., Indo Am. J. P. Sci*, no. 06, p. 6, 2019, [Online]. Available: http://www.iajps.com

[19] T. K. Gayen, M. A. Ali, and S. G. Warkar, “Carboxymethyl tamarind kernel gum bio-hydrogel for soil amendment and micronutrient release in sustainable agricultural technologies,” *Polymer Bulletin*, vol. 82, no. 17, pp. 11857–11883, Nov. 2025, doi: 10.1007/s00289-025-05995-x.

[20] Kajal, R. Kumar, P. Meena, and S. G. Warkar, “Development and characterization of pH-responsive CMTKG/PAM/PEG hydrogel for oral administration of etophylline,” *Colloid Polym. Sci.*, vol. 301, no. 11, pp. 1313–1323, Nov. 2023, doi: 10.1007/s00396-023-05152-8.

[21] M. Ashraf *et al.*, “Graduation project on: Sustainable Valorization of Tamarind Waste: Synthesis and Application of Carboxymethyl Tamarind as an Eco-Friendly Tamarind Kernel Thickener for Printing and other Applications Under the Supervision of.”

[22] T. Topală, A. Bodoki, L. Oprean, and R. Oprean, “Bovine serum albumin interactions with metal complexes,” *Clujul Medical*, vol. 87, no. 4, p. 5, 2014, doi: 10.15386/cjmed-357.

[23] S. Behera *et al.*, “Selective Binding of Bovine Serum Albumin (BSA): A Comprehensive Review,” 2023, *AMG Transcend Association*. doi: 10.33263/BRIAC136.555.

[24] A. Ravindran, A. Singh, A. M. Raichur, N. Chandrasekaran, and A. Mukherjee, “Studies on interaction of colloidal Ag nanoparticles with Bovine Serum Albumin (BSA),” *Colloids Surf. B Biointerfaces*, vol. 76, no. 1, pp. 32–37, Mar. 2010, doi: 10.1016/j.colsurfb.2009.10.005.

[25] Q. Ma, P. J. Shuler, C. W. Aften, and Y. Tang, “Theoretical studies of hydrolysis and stability of polyacrylamide polymers,” *Polym. Degrad. Stab.*, vol. 121, pp. 69–77, Nov. 2015, doi: 10.1016/j.polymdegradstab.2015.08.012.

[26] C. Zhou and Q. Wu, “A novel polyacrylamide nanocomposite hydrogel reinforced with natural chitosan nanofibers,” *Colloids Surf. B Biointerfaces*, vol. 84, no. 1, pp. 155–162, May 2011, doi: 10.1016/j.colsurfb.2010.12.030.

[27] J. Kundu, L. A. Poole-Warren, P. Martens, and S. C. Kundu, “Silk fibroin/poly(vinyl alcohol) photocrosslinked hydrogels for delivery of macromolecular drugs,” *Acta Biomater.*, vol. 8, no. 5, pp. 1720–1729, 2012, doi: 10.1016/j.actbio.2012.01.004.

[28] A. M. F. Alhalawani, D. J. Curran, D. Boyd, and M. R. Towler, “The role of poly(acrylic acid) in conventional glass polyalkenoate cements,” Apr. 01, 2016, *Walter de Gruyter GmbH*. doi: 10.1515/polyeng-2015-0079.

[29] S. Das, C. Krishi Viswavidyalaya, and A. B. Sharangi, “Madagascar periwinkle (Catharanthus roseus L.): Diverse medicinal and therapeutic benefits to humankind,” *~ 1695 ~ Journal of Pharmacognosy and Phytochemistry*, vol. 6, no. 5, pp. 1695–1701, 2017.

[30] V. Shoba, “Ethnobotanical and Phyto Pharmacological Activities of Madagascar periwinkle (Catharanthus Roseus)-A Detailed Review, Indo Am,” *J. P. Sci*, no. 12, pp. 4979–4986, 2017, doi: 10.5281/zenodo.1342748.

[31] N. Nejat, A. Valdiani, D. Cahill, Y. H. Tan, M. Maziah, and R. Abiri, “Ornamental exterior versus therapeutic interior of Madagascar periwinkle (Catharanthus roseus): The two faces of a versatile herb,” Jan. 15, 2015, *Hindawi Publishing Corporation*. doi: 10.1155/2015/982412.

[32] “CuO PAPER”.

[33] I. H. Bhuiyan *et al.*, “Green Synthesis and Characterization of Copper Oxide (CuO) Nanoparticles Using Mesua ferrea Leaf Extract and Evaluation of Biological Activities,” *ChemistrySelect*, vol. 10, no. 43, Nov. 2025, doi: 10.1002/slct.202503202.

[34] C. P. Pangestutia and N. Nazriati, “Green Synthesis, Characterization, and Antibacterial Activity of Copper Oxide Nanoparticles (CuO NPs) Using Papaya Leaf (Carica papaya L.) Extract as a Capping Agent,” *Jurnal Riset Kimia*, vol. 17, no. 1, pp. 35–49, Mar. 2026, doi: 10.25077/jrk.v17i1.866.

[35] Y. Li, M. Kröger, and W. K. Liu, “Endocytosis of PEGylated nanoparticles accompanied by structural and free energy changes of the grafted polyethylene glycol,” *Biomaterials*, vol. 35, no. 30, pp. 8467–8478, 2014, doi: 10.1016/j.biomaterials.2014.06.032.

[36] P. Gauba and A. Saxena, “Ciprofloxacin properties, impacts, and remediation,” 2023, *CABI International*. doi: 10.1079/cabireviews.2023.0005.

[37] G. A. Islan and G. R. Castro, “Tailoring of alginate-gelatin microspheres properties for oral Ciprofloxacin-controlled release against Pseudomonas aeruginosa,” *Drug Deliv.*, vol. 21, no. 8, pp. 615–626, Dec. 2014, doi: 10.3109/10717544.2013.870257.

[38] I. Rani, S. G. Warkar, and A. Kumar, “Nano ZnO embedded poly (ethylene glycol) diacrylate cross-linked carboxymethyl tamarind kernel gum (CMTKG)/poly (sodium acrylate) composite hydrogels for oral delivery of ciprofloxacin drug and their antibacterial properties,” *Mater. Today Commun.*, vol. 35, Jun. 2023, doi: 10.1016/j.mtcomm.2023.105635.

[39] F. Sabbagh and I. I. Muhamad, “Acrylamide-based hydrogel drug delivery systems: Release of Acyclovir from MgO nanocomposite hydrogel,” *J. Taiwan Inst. Chem. Eng.*, vol. 72, pp. 182–193, Mar. 2017, doi: 10.1016/j.jtice.2016.11.032.

[40] Y. Wang *et al.*, “Repair of degenerative nucleus pulposus by polyphenol nanosphere-encapsulated hydrogel gene delivery system,” *Biomaterials*, vol. 298, Jul. 2023, doi: 10.1016/j.biomaterials.2023.122132.

[41] A. Parvaresh, Z. Izadi, H. Nemati, H. Derakhshankhah, and M. Jaymand, “Redox- and pH-responsive alginate-based magnetic hydrogel: ‘Smart’ drug delivery and protein corona studies,” *J. Mol. Liq.*, vol. 382, Jul. 2023, doi: 10.1016/j.molliq.2023.121990.

[42] H. Shen *et al.*, “A matrix metalloproteinase-sensitive hydrogel combined with photothermal therapy for transdermal delivery of deferoxamine to accelerate diabetic pressure ulcer healing,” *Chinese Chemical Letters*, vol. 35, no. 12, Dec. 2024, doi: 10.1016/j.cclet.2024.110283.

[43] A. Sajid *et al.*, “Synthesis of bimetallic oxides (SrO-CoO) nanoparticles decorated polyacrylamide hydrogels for controlled drug release and wound healing applications,” *Int. J. Biol. Macromol.*, vol. 274, Aug. 2024, doi: 10.1016/j.ijbiomac.2024.133194.

[44] A. Gupta, S. Yadav, N. Rani, K. Gupta, and K. Saini, “Degradation of toxic methylene blue dye with Zinc oxide (ZnO) nanoparticles synthesized by leaf extract of Madagascar periwinkle plant,” *Biomass Convers. Biorefin.*, vol. 15, no. 17, pp. 24629–24640, Sep. 2025, doi: 10.1007/s13399-024-05711-1.

[45] S. M. Taghizadeh, A. Ebrahiminezhad, M. J. Raee, H. Ramezani, A. Berenjian, and Y. Ghasemi, “A Study of l-Lysine-Stabilized Iron Oxide Nanoparticles (IONPs) on Microalgae Biofilm Formation of Chlorella vulgaris,” *Mol. Biotechnol.*, vol. 64, no. 6, pp. 702–710, Jun. 2022, doi: 10.1007/s12033-022-00454-8.

[46] T. Kumari, Nitin, P. Meena, and S. G. Warkar, “Development and evaluation of gelatin/polyacrylamide/carboxymethyl tamarind kernel gum hydrogel for delivery of ampicillin sodium,” *Indian Journal of Chemical Technology*, vol. 31, no. 5, pp. 681–690, Sep. 2024, doi: 10.56042/ijct.v31i5.10942.

[47] Kajal, R. Kumar, P. Meena, and S. G. Warkar, “Development and characterization of pH-responsive CMTKG/PAM/PEG hydrogel for oral administration of etophylline,” *Colloid Polym. Sci.*, vol. 301, no. 11, pp. 1313–1323, Nov. 2023, doi: 10.1007/s00396-023-05152-8.

[48] P. Meena, P. Singh, and S. G. Warkar, “Tailoring pH-sensitive carboxymethyl tamarind kernel gum-based hydrogel for an efficient delivery of hydrophobic drug indomethacin,” *Int. J. Biol. Macromol.*, vol. 280, Nov. 2024, doi: 10.1016/j.ijbiomac.2024.136029.

[49] R. Khan *et al.*, “Synthesis of Chemically Cross-Linked pH-Sensitive Hydrogels for the Sustained Delivery of Ezetimibe,” *Gels*, vol. 8, no. 5, pp. 1–17, 2022, doi: 10.3390/gels8050281.

[50] N. Shahid *et al.*, “Ph-responsive nanocomposite based hydrogels for the controlled delivery of ticagrelor; in vitro and in vivo approaches,” *Int. J. Nanomedicine*, vol. 16, pp. 6345–6366, 2021, doi: 10.2147/IJN.S330186.

[51] G. Verma and M. Mishra, “DEVELOPMENT AND OPTIMIZATION OF UV-VIS SPECTROSCOPY-A REVIEW,” *Govinda et al. World Journal of Pharmaceutical Research*, vol. 7, 2018, doi: 10.20959/wjpr201811-12333.

[52] M. K. Kiteto and C. A. Mecha, “Insight into the Bouguer-Beer-Lambert Law: A review”, doi: 10.37256/fce.5220245325.

[53] H. Soonmin, “Investigation of Optical Properties of Thin Films by Means of UV-visible Spectrophotometer: A Review,” in *New Frontiers in Physical Science Research Vol. 5*, B P International (a part of SCIENCEDOMAIN International), 2022, pp. 66–82. doi: 10.9734/bpi/nfpsr/v5/4498e.

[54] H. Kaur, B. Rana, D. Tomar, S. Kaur, and K. C. Jena, “Fundamentals of ATR-FTIR Spectroscopy and Its Role for Probing In-Situ Molecular-Level Interactions,” in *Progress in Optical Science and Photonics*, vol. 13, Springer, 2021, pp. 3–37. doi: 10.1007/978-981-33-6084-6_1.

[55] K. L. Bunker *et al.*, “TEM and FESEM: The right combination for enhanced particle characterization,” in *Microscopy and Microanalysis*, Aug. 2008, pp. 580–581. doi: 10.1017/S1431927608083682.

[56] B. Lewczuk and N. Szyryńska, “Field-emission scanning electron microscope as a tool for large-area and large-volume ultrastructural studies,” Dec. 01, 2021, *MDPI*. doi: 10.3390/ani11123390.

[57] R. Senthil Prabhu, R. Priyanka, M. Vijay, and G. R. Kaviya Vikashini, “Field Emission Scanning Electron Microscopy (Fesem) with A Very Big Future in Pharmaceutical Research,” *Research Article | Pharmaceutical Sciences | OA Journal | MCI Approved | Index Copernicus*, vol. 11, no. 2, pp. 2321–3272, 2021, doi: 10.21276/ijpbs.2021.11.2.21.

[58] A. Chauhan, “Powder XRD Technique and its Applications in Science and Technology,” *J. Anal. Bioanal. Tech.*, vol. 5, no. 6, 2014, doi: 10.4172/2155-9872.1000212.

[59] K. Khushbu, S. G. Warkar, and N. Thombare, “Zinc micronutrient-loaded carboxymethyl tamarind kernel gum-based superabsorbent hydrogels: controlled release and kinetics studies for agricultural applications,” *Colloid Polym. Sci.*, vol. 299, no. 7, pp. 1103–1111, Jul. 2021, doi: 10.1007/s00396-021-04831-8.

[60] R. Abdelkader and B. Mohammed, “Green synthesis of cationic polyacrylamide composite catalyzed by an ecologically catalyst clay called maghnite-H+ (Algerian MMT) under microwave irradiation,” *Bulletin of Chemical Reaction Engineering and Catalysis*, vol. 11, no. 2, pp. 170–175, 2016, doi: 10.9767/bcrec.11.2.543.170-175.

[61] T. F. M. Oudemans, J. J. Boon, and R. E. Botto, “FTIR AND SOLID-STATE 13 C CP/MAS NMR SPECTROSCOPY OF CHARRED AND NON-CHARRED SOLID ORGANIC RESIDUES PRESERVED IN ROMAN IRON AGE VESSELS FROM THE NETHERLANDS*,” 2007.

[62] A. Varughese, R. Kaur, and P. Singh, “Green Synthesis and Characterization of Copper Oxide Nanoparticles Using Psidium guajava Leaf Extract,” in *IOP Conference Series: Materials Science and Engineering*, IOP Publishing Ltd, Nov. 2020. doi: 10.1088/1757-899X/961/1/012011.

[63] L. Stagi *et al.*, “Modulating the poly-l-lysine structure through the control of the protonation–deprotonation state of l-lysine,” *Sci. Rep.*, vol. 12, no. 1, Dec. 2022, doi: 10.1038/s41598-022-24109-5.

[64] M. I. Nabila and K. Kannabiran, “Biosynthesis, characterization and antibacterial activity of copper oxide nanoparticles (CuO NPs) from actinomycetes,” *Biocatal. Agric. Biotechnol.*, vol. 15, pp. 56–62, Jul. 2018, doi: 10.1016/j.bcab.2018.05.011.

[65] H. N. Jayasimha, K. G. Chandrappa, P. F. Sanaulla, and V. G. Dileepkumar, “Green synthesis of CuO nanoparticles: A promising material for photocatalysis and electrochemical sensor,” *Sensors International*, vol. 5, Jan. 2024, doi: 10.1016/j.sintl.2023.100254.

[66] P. Yadav, S. G. Warkar, and A. Kumar, “A comparative analysis of carboxymethyl tamarind kernel gum-based hydrogels for ciprofloxacin delivery,” *Int. J. Biol. Macromol.*, vol. 282, Dec. 2024, doi: 10.1016/j.ijbiomac.2024.136569.

[67] H. Siddiqui, M. S. Qureshi, and F. Z. Haque, “Valuation of copper oxide (CuO) nanoflakes for its suitability as an absorbing material in solar cells fabrication,”

Optik (Stuttg)., vol. 127, no. 8, pp. 3713–3717, Apr. 2016, doi: 10.1016/j.ijleo.2015.12.133.

[68] M. Eltarahony, S. Zaki, and D. Abd-El-Haleem, "Concurrent synthesis of zero- and one-dimensional, spherical, rod-, needle-, and wire-shaped cuo nanoparticles by proteus mirabilis 10B," *J. Nanomater.*, vol. 2018, 2018, doi: 10.1155/2018/1849616.

[69] M. Yadollahi, I. Gholamali, H. Namazi, and M. Aghazadeh, "Synthesis and characterization of antibacterial carboxymethylcellulose/CuO bio-nanocomposite hydrogels," *Int. J. Biol. Macromol.*, vol. 73, no. 1, pp. 109–114, Feb. 2015, doi: 10.1016/j.ijbiomac.2014.10.063.

[70] F. BORAN and Ç. KARAKAYA, "Polyvinyl alcohol/CuO nanocomposite hydrogels: facile synthesis and long-term stability," *Balıkesir Üniversitesi Fen Bilimleri Enstitüsü Dergisi*, vol. 21, no. 2, pp. 512–530, Jun. 2019, doi: 10.25092/baunfbed.624392.

[71] V. Pawar, M. Dhanka, and R. Srivastava, "Cefuroxime conjugated chitosan hydrogel for treatment of wound infections," *Colloids Surf. B Biointerfaces*, vol. 173, pp. 776–787, Jan. 2019, doi: 10.1016/j.colsurfb.2018.10.034.

[72] N. Sedefoglu, S. Er, K. Veryer, Y. Zalaoglu, and F. Bozok, "Green synthesized CuO nanoparticles using macrofungi extracts: Characterization, nanofertilizer and antibacterial effects," *Mater. Chem. Phys.*, vol. 309, Nov. 2023, doi: 10.1016/j.matchemphys.2023.128393.

[73] F. Wahid, H. S. Wang, Y. S. Lu, C. Zhong, and L. Q. Chu, "Preparation, characterization and antibacterial applications of carboxymethyl chitosan/CuO nanocomposite hydrogels," *Int. J. Biol. Macromol.*, vol. 101, pp. 690–695, Aug. 2017, doi: 10.1016/j.ijbiomac.2017.03.132.

[74] S. Alinavaz, G. R. Mahdavinia, H. Jafari, M. Hazrati, and A. Akbari, "Hydroxyapatite (HA)-based hybrid bionanocomposite hydrogels: Ciprofloxacin delivery, release kinetics and antibacterial activity," *J. Mol. Struct.*, vol. 1225, Feb. 2021, doi: 10.1016/j.molstruc.2020.129095.

[75] “Asianjournalofchemistry”.

[76] Y. Zhang *et al.*, “Hyperbranched glycopolymers of 2-(α-D-Mannopyranose) ethyl methacrylate and N, N’-methylenebisacrylamide: Synthesis, characterization and multivalent recognitions with concanavalin A,” *Polymers (Basel).*, vol. 10, no. 2, Feb. 2018, doi: 10.3390/polym10020171.

[77] T. Kumari, Nitin, P. Meena, and S. G. Warkar, “Development and evaluation of gelatin/polyacrylamide/carboxymethyl tamarind kernel gum hydrogel for delivery of ampicillin sodium,” *Indian Journal of Chemical Technology*, vol. 31, no. 5, pp. 681–690, Sep. 2024, doi: 10.56042/ijct.v31i5.10942.

[78] E. Badetti *et al.*, “Interaction between copper oxide nanoparticles and amino acids: Influence on the antibacterial activity,” *Nanomaterials*, vol. 9, no. 5, May 2019, doi: 10.3390/nano9050792.

[79] D. S. El-Sayed, E. M. Tawfik, A. F. Elhusseiny, and A. El-Dissouky, “A perception into binary and ternary copper (II) complexes: synthesis, characterization, DFT modeling, antimicrobial activity, protein binding screen, and amino acid interaction,” *BMC Chem.*, vol. 17, no. 1, Dec. 2023, doi: 10.1186/s13065-023-00962-x.

[80] P. Yadav, S. G. Warkar, and A. Kumar, “Development of graphene oxide-incorporated biopolymer-carboxymethyl tamarind kernel gum-based hydrogel as an effective adsorbent for the sequestration of dye pollutants,” *Polym. Eng. Sci.*, vol. 64, no. 10, pp. 4816–4833, Oct. 2024, doi: 10.1002/pen.26883.

[81] D. Tada, T. Tanabe, A. Tachibana, and K. Yamauchi, “Drug release from hydrogel containing albumin as crosslinker,” *J. Biosci. Bioeng.*, vol. 100, no. 5, pp. 551–555, 2005, doi: 10.1263/jbb.100.551.

[82] Y. Kaptan, O. Karal-Yilmaz, B. Izbudak, B. Giray, B. Yilmaz, and A. Bal-Ozturk, “Preparation of tetracycline hydrochloride loaded chitosan/silk fibroin/ZnO antibacterial biocomposite hydrogel sponges for wound healing application,” *Journal of Polymer Research*, vol. 30, no. 2, Feb. 2023, doi: 10.1007/s10965-022-03435-2.

[83] E. Assadian, M. H. Zarei, A. G. Gilani, M. Farshin, H. Degampanah, and J. Pourahmad, “Toxicity of Copper Oxide (CuO) Nanoparticles on Human Blood Lymphocytes,” *Biol. Trace Elem. Res.*, vol. 184, no. 2, pp. 350–357, Aug. 2018, doi: 10.1007/s12011-017-1170-4.

[84] A. El-Trass, H. Elshamy, I. El-Mehasseb, and M. El-Kemary, “CuO nanoparticles: Synthesis, characterization, optical properties and interaction with amino acids,” *Appl. Surf. Sci.*, vol. 258, no. 7, pp. 2997–3001, Jan. 2012, doi: 10.1016/j.apsusc.2011.11.025.

[85] K. M. Sahu, A. Biswal, U. Manisha, and S. K. Swain, “Synthesis and drug release kinetics of ciprofloxacin from polyacrylamide/dextran/carbon quantum dots (PAM/Dex/CQD) hydrogels,” *Int. J. Biol. Macromol.*, vol. 269, Jun. 2024, doi: 10.1016/j.ijbiomac.2024.132132.

[86] J. Sultana, M. Salim Hossain, M. Shahdaat Bin Sayeed, S. M. Ashraful Islam, and M. Safiqul Islam, “Indian Journal of Novel Drug Delivery IJNDD An Official Publication of Karnataka Education and Scientific Society Modification of Ciprofloxacin HCl release from Povidone K-30 based Matrix as a Function of Avicel pH 101.”

[87] Z. Sayyar, G. R. Mahdavinia, and A. Khataee, “Dual-drug (Curcumin/Ciprofloxacin) loading and release from chitosan-based hydrogels embedded with magnetic Montmorillonite/Hyaluronic acid for enhancing wound healing,” *J. Biol. Eng.*, vol. 17, no. 1, Dec. 2023, doi: 10.1186/s13036-023-00385-1.

[88] N. Goonoo, A. Bhaw-Luximon, R. Ujoodha, A. Jhugroo, G. K. Hulse, and D. Jhurry, “Naltrexone: A review of existing sustained drug delivery systems and emerging nano-based systems,” Jun. 10, 2014, *Elsevier*. doi: 10.1016/j.jconrel.2014.03.046.

[89] N. H. Thang, T. B. Chien, and D. X. Cuong, “Polymer-Based Hydrogels Applied in Drug Delivery: An Overview,” Jul. 01, 2023, *Multidisciplinary Digital Publishing Institute (MDPI)*. doi: 10.3390/gels9070523.

[90] N. Rafique, M. Ahmad, M. U. Minhas, S. F. Badshah, N. S. Malik, and K. U. Khan, “Designing gelatin-based swellable hydrogels system for controlled delivery of salbutamol sulphate: characterization and toxicity evaluation,” *Polymer Bulletin*, vol. 79, no. 7, pp. 4535–4561, Jul. 2022, doi: 10.1007/s00289-021-03629-6.

[91] A. Paydayesh, L. Heleil, and A. Sh Dadkhah, “Preparation and application of poly (hydroxyl ethyl methacrylate) nanocomposite hydrogels containing iron oxide nanoparticles as wound dressing,” *Polymers and Polymer Composites*, vol. 30, Jan. 2022, doi: 10.1177/09673911211063106.

APPENDICES

Conference details

Presented our research work at the ***"International Conference on Smart materials and Biodegradable chemical Alternatives"*** organized by International Network for Research and Innovation held on 7 June 2026 at Delhi, India.


Google Scholar
CERTIFICATE
OF PRESENTATION
INRI
International Conference on Smart Materials and Biodegradable Chemical Alternatives (ICSMBCA-26)
07th June 2026 | Delhi - India
THIS IS TO CERTIFY THAT
Nancy Sharma
affiliated with Delhi Technological University, Delhi, India has presented a paper titled
"CMTKG based Hydrogel incorporating Metal Oxide Nanoparticles for Drug Delivery Applications"
at the conference organized by the International Network for Research & Innovation held on 07th June 2026 at Delhi - India.
OPEN ACCESS
Organizing Committee Head
INRI
Authorizing Signature
INRI
DOAJ DIRECTORY OF OPEN ACCESS JOURNALS


Google Scholar
CERTIFICATE
OF PRESENTATION
INRI
International Conference on Smart Materials and Biodegradable Chemical Alternatives (ICSMBCA-26)
07th June 2026 | Delhi - India
THIS IS TO CERTIFY THAT
Rahul Panwar
affiliated with Delhi Technological University, Delhi, India has presented a paper titled
"CMTKG based Hydrogel incorporating Metal Oxide Nanoparticles for Drug Delivery Applications"
at the conference organized by the International Network for Research & Innovation held on 07th June 2026 at Delhi - India.
OPEN ACCESS
Organizing Committee Head
INRI
Authorizing Signature
INRI
DOAJ DIRECTORY OF OPEN ACCESS JOURNALS

Plagiarism Report

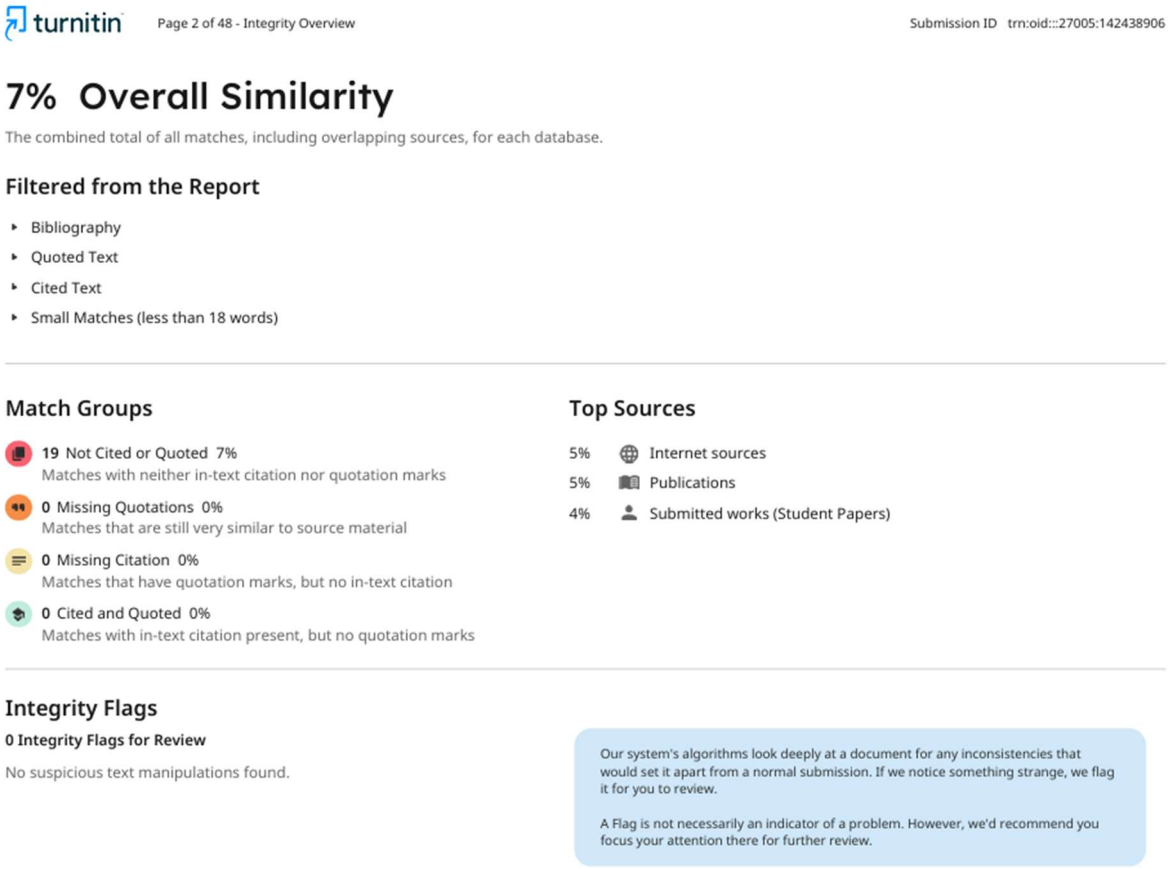

turnitin Page 2 of 48 - Integrity Overview Submission ID trn:oid:::27005:142438906

7% Overall Similarity

The combined total of all matches, including overlapping sources, for each database.

Filtered from the Report

- Bibliography
- Quoted Text
- Cited Text
- Small Matches (less than 18 words)

Match Groups

19 Not Cited or Quoted 7%
Matches with neither in-text citation nor quotation marks

0 Missing Quotations 0%
Matches that are still very similar to source material

0 Missing Citation 0%
Matches that have quotation marks, but no in-text citation

0 Cited and Quoted 0%
Matches with in-text citation present, but no quotation marks

Top Sources

5% Internet sources
5% Publications
4% Submitted works (Student Papers)

Integrity Flags

0 Integrity Flags for Review

No suspicious text manipulations found.

Our system's algorithms look deeply at a document for any inconsistencies that would set it apart from a normal submission. If we notice something strange, we flag it for you to review.

A Flag is not necessarily an indicator of a problem. However, we'd recommend you focus your attention there for further review.

AI Report

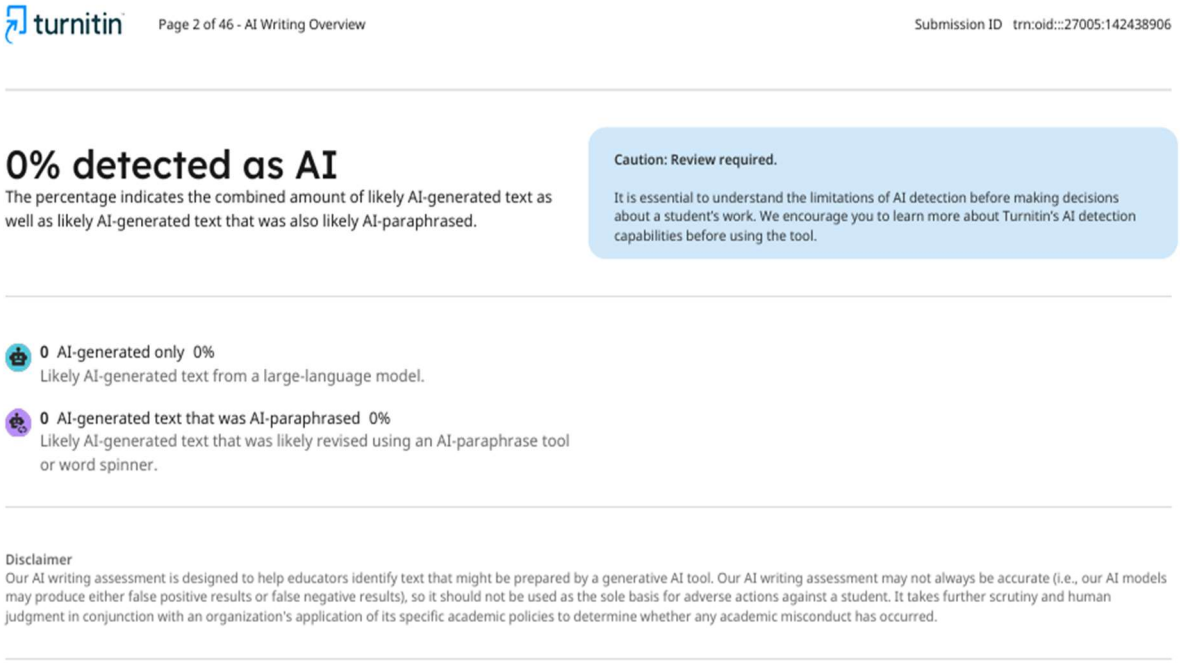

turnitin Page 2 of 46 - AI Writing Overview Submission ID trn:oid:::27005:142438906

0% detected as AI

The percentage indicates the combined amount of likely AI-generated text as well as likely AI-generated text that was also likely AI-paraphrased.

Caution: Review required.

It is essential to understand the limitations of AI detection before making decisions about a student's work. We encourage you to learn more about Turnitin's AI detection capabilities before using the tool.

0 AI-generated only 0%
Likely AI-generated text from a large-language model.

0 AI-generated text that was AI-paraphrased 0%
Likely AI-generated text that was likely revised using an AI-paraphrase tool or word spinner.

Disclaimer
Our AI writing assessment is designed to help educators identify text that might be prepared by a generative AI tool. Our AI writing assessment may not always be accurate (i.e., our AI models may produce either false positive results or false negative results), so it should not be used as the sole basis for adverse actions against a student. It takes further scrutiny and human judgment in conjunction with an organization's application of its specific academic policies to determine whether any academic misconduct has occurred.